The Astronomical Journal, 130:2625–2646, 2005 December

NEW OPTICAL AND NEAR-INFRARED SURFACE BRIGHTNESS FLUCTUATION MODELS. II. YOUNG AND INTERMEDIATE-AGE STELLAR POPULATIONS

G. Raimondo,[1] E. Brocato,[1] M. Cantiello,[1,2] and M. Capaccioli[3,4]

Received 2004 November 19; accepted 2005 August 15

ABSTRACT

We present theoretical surface brightness fluctuation (SBF) amplitudes for single-burst stellar populations of young and intermediate age (25 Myr $\leq t \leq$ 5 Gyr) and metallicities $Z = 0.0003$, 0.001, 0.004, 0.008, 0.01, 0.02, and 0.04. The fluctuation magnitudes and colors as expected in the Johnson-Cousins (*UBVRIJHK*) photometric system are provided. We pay attention to the contribution of thermally pulsating asymptotic giant branch (TP-AGB) stars. The sensitivity of the predicted SBF to changes in the mass-loss scenario along the TP-AGB phase is examined. Below 0.6–1 Gyr both optical and near-IR SBF models exhibit a strong dependence on age and mass loss. We also evaluate SBF amplitudes using Monte Carlo techniques to reproduce the random variation in the number of stars experiencing bright and fast evolutionary phases (red giant branch, AGB, TP-AGB). On these grounds we provide constraints on the faintest integrated flux of real stellar populations required to derive reliable and meaningful SBF measurements. We analyze a technique for deriving SBF amplitudes of star clusters from the photometry of individual stars and estimate the uncertainty due to statistical effects, which may impinge on the procedure. The first optical SBF measurements for 11 Large Magellanic Cloud (LMC) star-rich clusters—with ages ranging from a few megayears to several gigayears—are derived using *Hubble Space Telescope* observations. The measurements are compared to our SBF predictions, providing a good agreement with models of metallicity $Z = 0.0001$–0.01. Our results suggest that, for TP-AGB stars, a mass loss as a power-law function of the star luminosity is required in order to properly reproduce the optical SBF data of the LMC clusters. Finally, near-IR models have been compared to available data, thus showing that the general trend is well fitted. We suggest how to overcome the general problem of SBF models in reproducing the details of the near-IR SBF measurements of the Magellanic Cloud star clusters.

Key words: distance scale — galaxies: stellar content — globular clusters: general — open clusters and associations: general — stars: luminosity function, mass function

Online material: color figures

1. INTRODUCTION

The surface brightness fluctuation (SBF) technique (Tonry & Schneider 1988, hereafter TS88) is one of the most powerful methods for deriving extragalactic distances for gas-free stellar systems. In the last decade, the SBF technique has proven to be effective in estimating distances as far as 50 Mpc, and even larger, using ground-based observations (e.g., Tonry et al. 2001; Blakeslee et al. 2001; Mei et al. 2001; Liu et al. 2002) and out to distances exceeding 100 Mpc from space (Pahre et al. 1999; Jensen et al. 2003). Since the method has been primarily applied to elliptical galaxies and to the bulges of spirals, theoretical SBF studies have been mostly oriented toward old stellar systems ($t > 2$–5 Gyr; Worthey 1993; Buzzoni 1993; Liu et al. 2000; Blakeslee et al. 2001; Cantiello et al. 2003, hereafter Paper I).

Along with its ability in gauging distances, the SBF technique appears to be a very promising tool for investigating the evolution of unresolved stellar populations in distant galaxies. Attempts have been made to derive consistent estimations of age and metallicity for samples of galaxies from SBF measurements (Brocato et al. 1998; Liu et al. 2000, 2002; Blakeslee et al. 2001; Paper I; Raimondo et al. 2004). However, even in galaxies dominated by old stars, disregarding the effect of the contribution by possible intermediate-age and young stellar populations ($t < 2$–5 Gyr) may be hazardous. The presence of different stellar populations at different galactocentric distances, revealed by integrated colors and spectral index radial gradients, indicates that elliptical galaxies are mostly composite stellar systems (e.g., Pagel & Edmunds 1981). SBF gradient measurements support this view (Sodemann & Thomsen 1995; Cantiello et al. 2005). Relatively young He-burning and/or asymptotic giant branch (AGB) stars may contribute to the brightest part of the galaxy luminosity function (LF). Because the major contribution to the SBF signal comes from high-luminosity stars, it is relevant to know how SBF amplitudes change by lowering the age of the stellar system down to a few million years, in those photometric bands in which the SBF signal is mostly affected by the presence of young and intermediate-age stellar populations.

Before facing the problem of finding the age and metallicity of possibly mixed stellar populations in remote galaxies using SBFs, their capability as a population tracer has to be proven and carefully tested on stellar systems of known distance, age, and metallicity. Then, once calibrated on resolved Galactic and Local Group stellar populations, SBFs can become a valuable tool in the analysis of the stellar content in galaxies, where crowding and distance hamper studies made with the classical color-magnitude diagram (CMD) technique.

The SBF technique has also been recognized as effective in constraining stellar evolution theory. In a previous paper (Paper I) we showed that the SBFs of old populations are sensitive to the number of very bright stars evolving along the early AGB

[1] INAF–Osservatorio Astronomico di Teramo, Via M. Maggini, I-64100 Teramo, Italy; raimondo@oa-teramo.inaf.it, brocato@oa-teramo.inaf.it, cantiello@oa-teramo.inaf.it.

[2] Dipartimento di Fisica "E.R. Caianiello," Università di Salerno and INFN, Sezione di Napoli, Gruppo Collegato di Salerno, Via S. Allende, I-84081 Baronissi, Salerno, Italy.

[3] Dipartimento di Scienze Fisiche, Università di Napoli Federico II, Complesso Monte S. Angelo, Via Cintia, I-80126 Naples, Italy; capaccioli@na.astro.it.

[4] INAF–Osservatorio Astronomico di Capodimonte, Via Moiariello 16, I-80131 Naples, Italy.

and thermally pulsating AGB (TP-AGB). In young stellar populations—but old enough to have stars in these stages—stochastic fluctuations of the number of AGB stars (as triggered by mass-loss processes and evolutionary timescale) are expected to have even more relevance in predicting SBF amplitudes. If this is confirmed, the SBF technique can also provide a new and unexplored way for improving our understanding of physical processes at work in AGB stars of intermediate mass ($m \sim 5\ M_{\odot}$).

In the last few years, a large effort toward improving stellar evolution models has been made in order to reproduce both the details of AGB star evolution (Straniero et al. 1997; Pols & Tout 2001) and the evolution of "normal" stars. New physics experiments have advanced our knowledge of nuclear reaction rates inside stars and the equation of state of stellar matter in critical conditions. Updated and homogeneous evolutionary track databases, reproducing the observed CMDs of young and intermediate-age stellar populations in detail (e.g., Brocato et al. 2003), are now available (Girardi et al. 2000; Castellani et al. 2003; Marigo et al. 2003; Pietrinferni et al. 2004, hereafter P04). Therefore, very accurate SBF amplitudes can now be computed in this age range.

Pioneering work on SBFs from young simple stellar populations (SSPs) has been carried out by Gonzalez et al. (2003; Gonzalez et al. 2004, hereafter G04) in the near-IR (NIR) and by Raimondo et al. (2003) in the optical regime. In the present paper we evaluate SBF amplitudes expected from SSPs younger than 5 Gyr, with metallicities from $Z = 0.0003$ to 0.04. Much attention is devoted to a simulation of the TP phase and its uncertainties by evaluating changes of chemical composition, stellar temperature, and the whole structure of TP-AGB stars as prescribed by Wagenhuber & Groenewegen (1998, hereafter WG98). Mass-loss processes complicate enormously the modeling of TP-AGB star observational properties.

This complex picture is expected to have a huge impact on the SBF behavior for intermediate-age stellar populations. In turn, SBF magnitudes and colors could be decisive in putting constraints on the evolution of AGB stars, e.g., the efficiency of mass loss, in stellar systems with known age and metallicity, since they are extremely efficient in mapping the properties of very bright stars in the population (Paper I).

In order to test our predictions, we select a sample of 11 star clusters of the Large Magellanic Cloud (LMC). For seven such clusters the estimated age is within the range studied here; the others are as old as the Galactic globular clusters (GGCs). Optical SBF measurements are derived using the photometry of resolved stars from high-resolution images of each cluster, as obtained with the Wide Field Planetary Camera 2 (WFPC2) on board the *Hubble Space Telescope* (*HST*).

The paper is organized as follows: A description of inputs of the stellar population synthesis code is presented in § 2. The methods for computing SBF amplitudes and stochastic effects due to the number of stars in the population are presented in §§ 3 and 3.1. SBF predictions are shown as a function of the TP-AGB stars mass-loss rate in § 3.2 and of metallicity in § 3.3. We derive the optical SBF measurements of the LMC star clusters in § 4 and present a comparison with models in § 5, together with a discussion on NIR SBFs. A summary and the final conclusions end the paper (§ 6).

2. THEORETICAL FRAMEWORK

In order to compute SBF amplitudes, we use the stellar population synthesis code described in Brocato et al. (1999, 2000). Here we only recall that the code starts directly from stellar evolutionary tracks and relies on the Monte Carlo technique for populating the initial mass function (IMF). The former property helps to avoid problems in the mass bin or luminosity bin procedures, which may affect the use of isochrones. The latter property allows us to take into account stochastic effects due to the number of stars in the stellar system, even for SBF amplitudes. If we deal with star clusters and undersampled stellar systems, stochastic fluctuations of the number of bright stars may affect integrated quantities (e.g., Santos & Frogel 1997; Brocato et al. 1999). The procedure used here takes these effects directly into account.

The present SSP models rely on the evolutionary track database by P04. All the evolutionary phases, from the main sequence (MS) up to the AGB, are covered by models. In particular, the AGB evolution runs up to the onset of the first thermal pulse or to the carbon ignition. We selected stellar evolutionary models with metallicities $Z = 0.0003$, 0.001, 0.004, 0.008, 0.01, 0.02, and 0.04, computed by adopting a solar-scaled metal distribution with an enrichment law of $\Delta Y/\Delta Z \simeq 1.4$.

In spite of the numerous improvements in the accuracy and precision of stellar evolutionary models, only a few tracks provide a detailed and full evolution along the TP-AGB phase (e.g., Straniero et al. 1997; Herwig et al. 1997; Pols & Tout 2001). Moreover, not all of them homogeneously cover the wide range of chemical compositions and stellar masses needed to investigate resolved and unresolved stellar populations. Since bright stars play a relevant role in determining SBFs, the TP-AGB phase cannot be neglected. We devoted particular care in including this evolutionary phase in our simulations. For the sake of readability, the discussion and details on how we treat TP-AGB stars are presented in Appendix A.

In the present paper, color–effective temperature ($T_{\rm eff}$) relations come from the semiempirical compilation by Westera et al. (2002), which is an updated version of the library by Lejeune et al. (1997). A Scalo-like IMF (Scalo 1998) is assumed for stellar masses in the interval $m = 0.1$–$10\ M_{\odot}$. Note that the upper mass limit corresponds to the highest mass evolving off the MS in the youngest population we considered, i.e., $t \sim 25$ Myr. All the more massive stars are expected to explode as supernovae, since their quiescent nuclear burning lifetime is as long as a few million years.

By means of Monte Carlo techniques, $N_{\rm sim} = 5000$ *independent* simulations are computed for each set of SSP parameters, i.e., age (t) and metallicity (Z). The total mass of each simulation is typically $\mathcal{M} \simeq 10^4\ M_{\odot}$, unless explicitly stated otherwise. The explored age range is 25 Myr $\leq t \leq$ 5 Gyr.[5] As an example of one of the 5000 simulations, in Figure 1 we report the synthetic CMDs of the simulated stellar populations, for a few selected ages, in the theoretical ($\log L/L_{\odot}$, $\log T_{\rm eff}$)-plane.

3. SBF AMPLITUDES

In this section we present two different methods for computing SBFs. We discuss in detail their analogies with observations and investigate stochastic effects on SBF amplitudes, caused by the discrete nature of the number of stars in stellar systems. The impact of bright and rare TP-AGB stars on SBFs is also presented.

The *standard* procedure we developed to calculate SBFs has already been presented in Paper I. It is based on the following equation, valid in the Gaussian statistics regime, i.e., for a high number of stars (TS88):

$$\bar{M}_X = -2.5 \log \bar{F}_X = -2.5 \log \left[\frac{\left\langle (F_X - \langle F_X \rangle)^2 \right\rangle}{\langle F_X \rangle} \right], \quad (1)$$

[5] At the time of publication, models fully consistent with the present theoretical scenario for ages larger than 5 Gyr, and for all metallicities presented here, are available at the Web site http://www.oa-teramo.inaf.it/SPoT. These old-age models will be discussed in detail in a forthcoming paper.

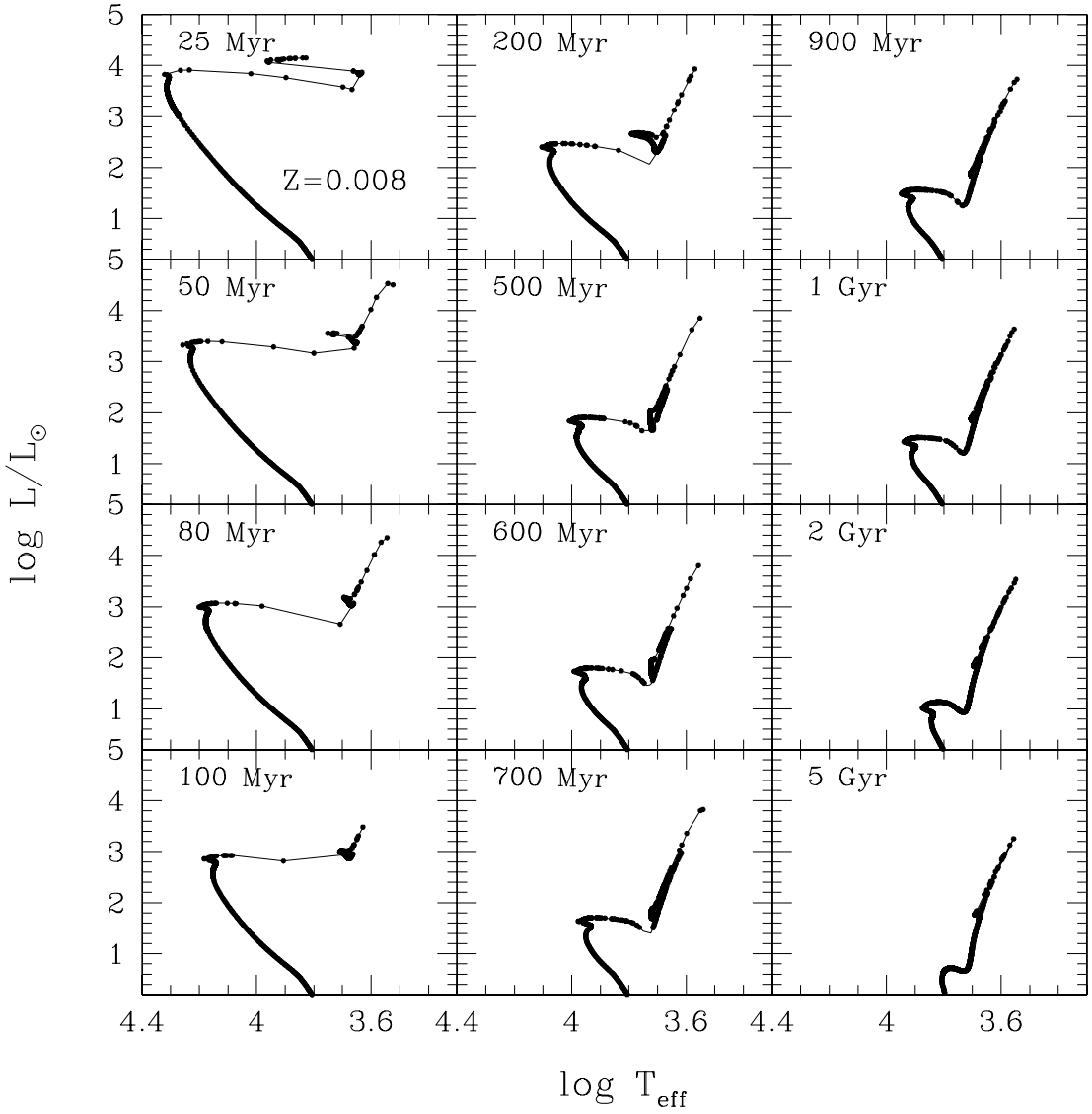

FIG. 1.—Sample of synthetic $\log(L/L_\odot)$ vs. $\log T_{\rm eff}$ diagrams for the labeled ages and $Z = 0.008$. In each panel one of the 5000 synthetic CMDs used to compute the SBFs is plotted (*circles*); the line represents the isochrone. A B1 mass-loss rate is assumed (see text and Appendix A).

where $\bar{F}_X$ is the flux fluctuation in the generic photometric filter X and F_X and $\langle F_X \rangle$ are respectively the total flux of each simulation and the mean total flux averaged over $N_{\rm sim}$ simulations, i.e.,

$$F_X \equiv F_X^j = \sum_{i=1}^{N_{\rm star}} f_i(X), \quad j = 1,\ N_{\rm sim}, \tag{2}$$

where $f_i(X)$ corresponds to the absolute flux of the ith star populating the jth simulation and

$$\langle F_X \rangle = \frac{\sum_{j=1}^{N_{\rm sim}} F_X^j}{N_{\rm sim}}. \tag{3}$$

For the sake of clarity, in this section absolute SBF amplitudes derived from equation (1) are indicated as $\bar{M}_X^{\rm std}$. As stated in Paper I, there is a close correspondence between the standard procedure and the way of measuring SBFs for unresolved stellar populations. In fact, the integrated energy flux F_X^j corresponds to the flux measured in a single pixel of a galaxy CCD image (if both seeing and population mixture are neglected).

When $N_{\rm sim}$ is equal to 5000, $\bar{M}_X^{\rm std}$ reaches the asymptotic value ($\bar{M}_X^{\rm std,\,as}$). Note that $\bar{M}_X^{\rm std}$ runs very quickly (after a few hundred simulations) toward $\bar{M}_X^{\rm std,\,as}$ (Appendix B), and the uncertainties are reduced ($\simeq$0.05 mag; Paper I). The asymptotic value has the same physical meaning as the classical SBF predictions in the literature (e.g., Worthey 1993; Buzzoni 1993; Liu et al. 2000; Blakeslee et al. 2001; G04).

For spatially resolved star clusters, we can apply another technique for measuring SBFs. It was first introduced by Ajhar & Tonry (1994, hereafter AT94) and is based on individual star photometry. By means of our method of computing SSP models and integrated properties, we can provide SBF predictions for each jth simulation by directly applying the definition of an SBF as introduced by TS88 (their eqs. [7]–[9]):

$$\bar{M}_X^{{\rm RS},\,j} = -2.5 \log \left[\frac{\sum_{i=1}^{N_{\rm star}} f_i(X)^2}{\sum_{i=1}^{N_{\rm star}} f_i(X)} \right], \quad j = 1,\ N_{\rm sim}. \tag{4}$$

Note that $\bar{M}_X^{{\rm RS},\,j}$ corresponds to the SBF obtained using the photometry of all stars in a cluster and directly relies on the Poissonian

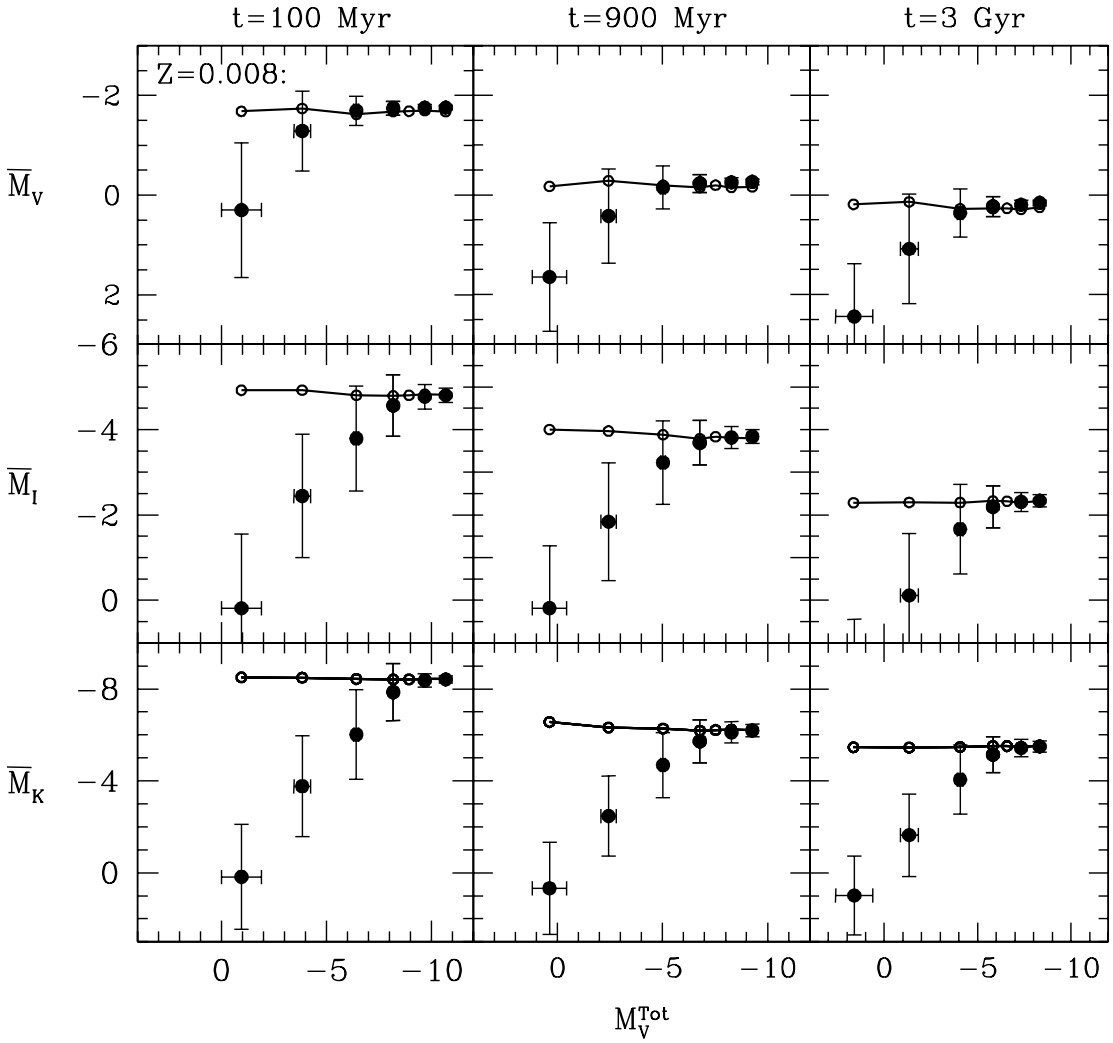

FIG. 2.—SBF absolute magnitudes as a function of the integrated absolute magnitude $M_V^{\rm tot}$. The solid lines and open circles represent the asymptotic SBF ($\bar{M}_X^{\rm std,as}$; eq. [1]). Filled circles represent $\bar{M}_X^{\rm RS}$ obtained from eq. (5) (see text). The adopted metallicity and ages are labeled.

statistics. The mean SBF magnitude averaged over $N_{\rm sim} = 5000$ independent simulations is

$$\bar{M}_X^{\rm RS} = \frac{\sum_{j=1}^{N_{\rm sim}} \bar{M}_X^{{\rm RS},j}}{N_{\rm sim}}, \qquad (5)$$

and the SBF statistical uncertainties can be derived as the standard deviation of the $\bar{M}_X^{{\rm RS},j}$ distribution. In the following, this procedure for computing SBFs is indicated as the RS (resolved systems) procedure.

3.1. *Statistical Effects*

In principle, the two procedures should provide very similar results. In practice, this is only true if the number of stars included in the jth simulation is large enough to populate all the evolutionary phases (i.e., if the Poisson statistics coincides with the Gaussian; TS88; Paper I). Hence, in order to analyze star cluster SBF magnitudes and to properly compare models with observations, it is crucial to investigate the dependence of SBF amplitudes on quantities related to the number of stars in the population. In the following we present a careful analysis of the statistical effects on SBF predictions. Although the analysis is specifically performed for star clusters, the technique we developed can be applied to any spatially resolved population.

For fixed age and metallicity, variations of the total number of stars among clusters result in a variation of the cluster total V magnitude ($M_V^{\rm tot}$). This is an observational quantity related to the number of stars included in the stellar population. We computed SBF amplitudes by adopting both procedures (the standard procedure [eq. (1)] and the RS procedure [eq. (5)]) and varying the SSP integrated absolute magnitude ($M_V^{\rm tot}$) from $M_V^{\rm tot} \simeq -1$ to -11 mag, a range larger than that observed for LMC clusters. This corresponds to varying the total mass of the population from $\mathcal{M}_{\rm tot} \sim 10^2$ to $\sim 10^5$ $M_\odot$. As usual, for each set of parameters (t, Z) we computed $N_{\rm sim}$ *independent* simulations.

Figure 2 shows the behavior of $\bar{M}_X^{\rm std,as}$ in the V, I, and K bands as a function of $M_V^{\rm tot}$ (*solid line*, *open circles*). Models for three different ages, $t = 100$ Myr, 900 Myr, and 3 Gyr, and $Z = 0.008$ are displayed. From all the panels it is evident that asymptotic SBF amplitudes ($\bar{M}_X^{\rm std,as}$) are stable within 0.1 mag in the wide range of $M_V^{\rm tot}$. In other words, independently of the cluster mass (luminosity), fluctuation amplitudes computed over 5000 simulations with the standard procedure predict nearly constant values.

SBF amplitudes resulting from the RS procedure ($\bar{M}_X^{\rm RS}$) are plotted as filled circles in Figure 2. The uncertainties due to stochastic fluctuations of the number of bright stars are directly evaluated as

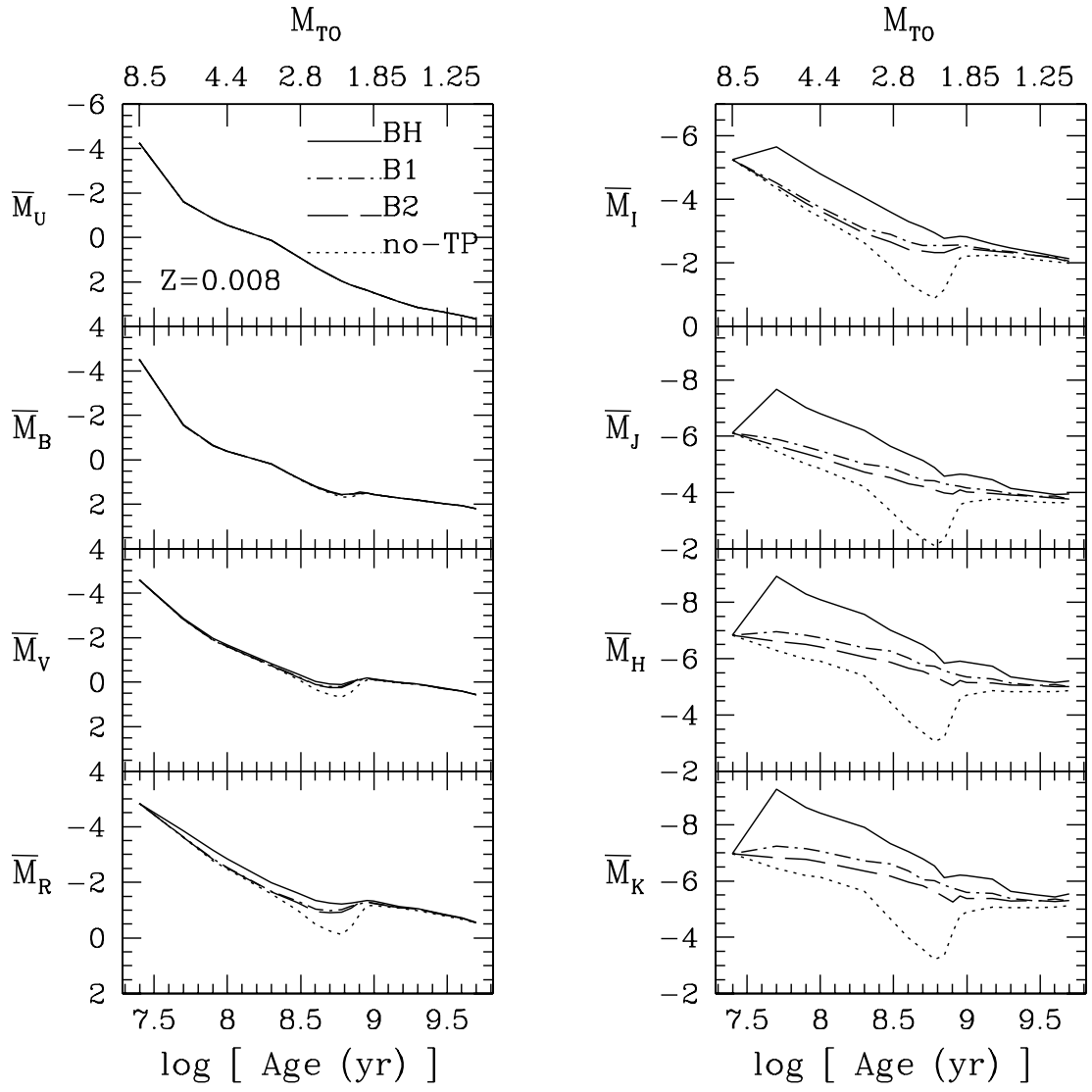

FIG. 3.—SBF magnitudes as a function of age, with fixed metallicity ($Z = 0.008$). Dotted lines correspond to models computed neglecting the TP-AGB phase (no-TP). Models including TP stars are plotted for three different mass-loss rates: BH models (*solid lines*), B1 models (*dot-dashed lines*), and B2 models (*long-dashed lines*). The MSTO masses (M_{TO}) at selected ages are also labeled.

the standard deviation of the $\bar{M}_X^{RS}$ distribution and plotted as 1 σ error bars. It is worth noting that the $\bar{M}_X^{RS}$ versus M_V^{tot} behavior is similar to that shown by integrated colors (e.g., Santos & Frogel 1997; Brocato et al. 1999).

The difference between the SBF asymptotic value and that derived from equation (5) is larger in the NIR bands than in the blue bands, because in the optical bands the contribution of the sparsely populated red giant branch (RGB) and AGB is less important than that of the well populated MS. By increasing the total luminosity (i.e., increasing the SSP mass), the two procedures converge to the same SBF value, and the uncertainty due to stochastic effects decreases accordingly. This happens when each simulation is well populated in all post-MS evolutionary stages until the TP phase. The maximum value of M_V^{tot} ($M_V^{tot,max}$), for which the two procedures give the same results within uncertainties, slightly depends on the age, in the sense that the older the population, the fainter $M_V^{tot,max}$. It changes from $M_V^{tot,max} \simeq -6.5$ to -4.5 mag by varying the age from $t = 100$ Myr to 3 Gyr.

Since the two theoretical procedures reflect different ways of measuring SBFs, the last finding has a direct effect on observations. The condition $M_V^{tot} \lesssim M_V^{tot,max}$ must be satisfied when comparing classical (asymptotic) SBF predictions to measurements derived from single-star photometry. In relatively poorly populated stellar systems, the random occurrence of bright stars deeply affects the SBF and should be taken into account in the comparison with models (that is, $\bar{M}_X^{RS}$ should be preferred).

In the standard procedure (i.e., the one used to measure SBFs in galaxies) SBFs are derived using the integrated flux of a large number of "similar" but "uncorrelated" populations (i.e., similar but uncorrelated pixels). This ensures the asymptotic SBF value is reached, even taking into account a relatively small number of pixels (see Appendix B). For example, if a fraction of young populations is expected in a galaxy, simulations suggest that the effective number of pixels used in measuring SBFs should not be less than 2000, so as to reduce the uncertainties due to statistical effects. This constraint becomes less stringent if the mass density of the young population is $\gtrsim 10^4\ M_\odot$ pixel^{-1}; i.e., 500 pixels are expected to be enough to keep such uncertainties below 0.1 mag.

In conclusion, we find that SBF models (classical asymptotic models) well represent SBFs as observed in galaxies, while for SBFs measured from resolved stellar systems, caution is required when performing comparisons with models. In particular, when

comparing SBF predictions with SBF observations for star clusters or undersampled stellar populations, attention should be paid when taking into account uncertainties due to the stochastic occurrence of bright stars experiencing fast and luminous evolutionary phases.

3.2. *The Impact of TP-AGB Stars*

Being extremely bright and rare, TP-AGB stars are relevant to the determination of the SBFs of young/intermediate-age stellar populations. One of the processes that determines the luminosity and the duration of the TP phase is mass loss. There are different mass-loss scenarios to be adopted during the TP phase (see Appendix A for a detailed discussion). This is a critical assumption, because the mass-loss efficiency determines the number of very bright TP-AGB stars. In order to understand the effective (quantitative) impact of such stars on SBFs, we computed a set of models by varying only the mass-loss rate:

BH models.—Mild mass-loss rate (Baud & Habing 1983, hereafter BH83). The TP phase is well populated (eq. [A7]).

B1 models.—Moderate mass-loss rate (Blocker 1995, hereafter B95) and few stars in the TP phase (eq. [A8]).

B2 models.—High mass-loss rate (B95) and few stars in the TP phase (eq. [A9]).

No-TP models.—Huge (unreal) mass-loss rate and no stars in the TP phase.

Let us analyze the case of $Z = 0.008$, i.e., a metallicity expected to be representative of the young/intermediate-age LMC star clusters (Westerlund 1997) we use as observational counterparts in § 4. Figure 3 illustrates the time evolution of SBF predictions for the four assumptions of mass-loss rate. We find that SBFs in the *U*, *B*, and *V* bands are not significantly affected by TP-AGB star mass-loss processes, whereas for redder bands, from *R* to *K*, SBFs may change by more than 1 mag for models older than ∼50 Myr and younger than ∼1 Gyr. The former value corresponds to the appearance of the AGB in an SSP with the metallicity above (AGB phase transition); the latter is related to the appearance of the RGB (RGB phase transition; Renzini & Buzzoni 1986). In this age range, the cool AGB stars (including the TP-AGB) dominate the integrated bolometric light.

In no-TP models, the brightest objects in the SSP are early AGB stars, i.e., stars before the first thermal pulse. Thus, SBF amplitudes are less luminous and extremely sensitive to the appearance of the RGB. On the other hand, the BH model mass-loss rate is not very efficient, and the resulting relatively high number of TP stars has three consequences: (1) SBFs are the most luminous (within our four cases) at any age, (2) SBFs experience an evident jump, due to the occurrence of the AGB phase transition at $t \sim 50$ Myr, and (3) SBFs do not vary significantly at the RGB phase transition age. B1 and B2 models lie within the previous two extreme cases. Since B1 and B2 mass-loss rates exponentially depend on the star luminosity, mass loss is much more efficient in massive AGB stars (young SSPs, $t \lesssim 200$ Myr) than in low-mass AGB stars (old SSPs). Consequently, in young SSPs, the TP phase is less populated, thus bringing the SBF values toward the no-TP case.

For ages $t \gtrsim 1$ Gyr, AGB stars become less relevant in predicting SBFs, because the RGB tip is nearly as bright as the AGB tip but much more populated (by about a factor of 10). This is the main reason why the four curves appear to converge at older ages.

Fluctuation colors present a very similar behavior (Fig. 4), showing a high sensitivity to TP-AGB star mass-loss rate and to the phase transitions. Of course, SBF colors might be more effective for detecting the efficiency of the TP-AGB star mass-loss rate than fluctuation magnitudes, as a consequence of their independence from distance.

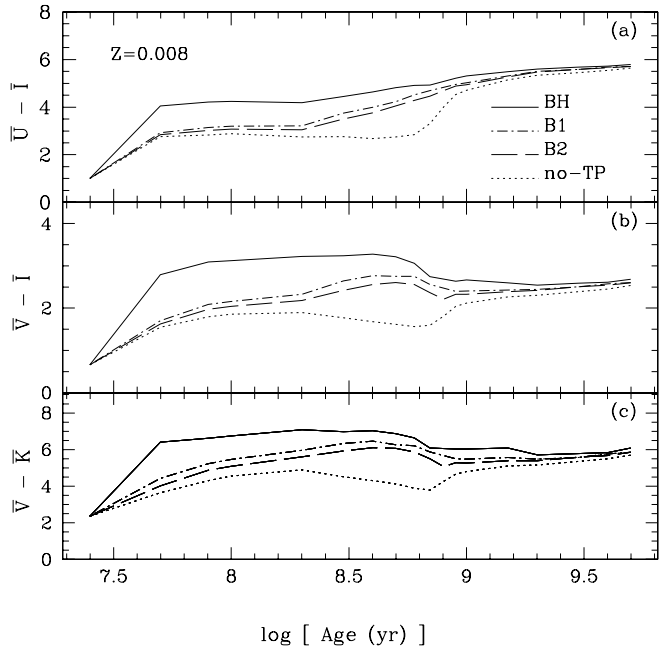

FIG. 4.—$\bar{U} - \bar{I}$, $\bar{V} - \bar{I}$, and $\bar{V} - \bar{K}$ fluctuation colors as a function of age, with fixed metallicity ($Z = 0.008$). Symbols are as in Fig. 3. The sensitivity to mass-loss rate assumed in modeling the TP-AGB phase is evident in the plotted colors.

The results in Figures 3 and 4 suggest at least two considerations: (1) the age of distant stellar systems can be inferred by measuring SBFs in blue bands (*U*, *B*, and *V*); and (2) SBFs measured in single-burst stellar populations could provide a tool to quantitatively evaluate the properties of TP-AGB stars, e.g., the expected number, luminosity, and mass loss.

3.3. *SBFs versus Metal Content*

Before concluding § 3 we discuss the SBF dependence on the chemical composition. Table 1 and Figure 5 report SBF amplitudes in Johnson-Cousins bands for different chemical compositions as a function of age. The input assumptions are the same as quoted at the beginning of § 3, and the adopted mass-loss scenario is B1. The reason for this choice is given in § 4. Table 1 lists age (col. [1]), absolute SBF magnitudes in various photometric filters (cols. [2]–[10]), absolute integrated *V* magnitude (col. [11]), and $V - I$ integrated color of the population (col. [12]). The SBF predictions are available online.[6]

The general trend of SBF magnitudes at different chemical compositions is similar to the one shown by models with $Z = 0.008$. As a general indication, we find that metal-poor ($Z \lesssim 0.001$) SSPs tend to have brighter SBFs in the optical bands. It is the opposite for NIR bands, since metal-rich populations show brighter SBFs, especially at an old age. This can be better understood if we remember that the RGB and AGB of metal-rich stars are cooler than the corresponding branches of metal-poor stars. Moreover, at young ages (several megayears) the appearance of AGB stars causes a sudden jump in the *mean* NIR SBF magnitude/color of the population. This is because SBFs are an extremely efficient measure of any fluctuation of the distribution of bright stars in the population. Since metal-rich (pre-AGB) bright stars are typically *redder* than similar metal-poor stars, correspondingly, the

[6] See http://www.oa-teramo.inaf.it/SPoT.

TABLE 1

SBF Amplitudes for B1 Models

Age (Gyr) (1)	$\bar{M}_U$ (2)	$\bar{M}_B$ (3)	$\bar{M}_V$ (4)	$\bar{M}_R$ (5)	$\bar{M}_I$ (6)	$\bar{M}_J$ (7)	$\bar{M}_H$ (8)	$\bar{M}_K$ (9)	$\bar{M}_L$ (10)	$M_V^{\rm tot}$ (11)	$V-I$ (12)
					$Z = 0.0003$, $Y = 0.245$						
0.025.....	−3.901	−3.010	−2.759	−2.794	−2.929	−3.435	−4.147	−4.231	−4.404	−8.872	−0.092
0.030.....	−3.639	−2.764	−2.584	−2.811	−3.275	−4.434	−5.461	−5.575	−5.783	−8.783	−0.063
0.050.....	−3.018	−2.473	−3.528	−4.597	−5.551	−7.078	−8.007	−8.128	−8.304	−8.746	0.276
0.080.....	−2.441	−2.041	−3.013	−4.051	−5.006	−6.555	−7.547	−7.675	−7.863	−8.572	0.240
0.100.....	−2.171	−1.867	−2.855	−3.888	−4.839	−6.392	−7.393	−7.523	−7.713	−8.515	0.252
0.200.....	−1.450	−1.326	−2.303	−3.284	−4.192	−5.711	−6.718	−6.845	−7.042	−8.312	0.292
0.300.....	−1.011	−0.990	−1.900	−2.863	−3.766	−5.329	−6.385	−6.522	−6.726	−8.187	0.320
0.400.....	−0.645	−0.761	−1.503	−2.377	−3.232	−4.759	−5.822	−5.959	−6.170	−8.121	0.323
0.500.....	−0.295	−0.632	−1.393	−2.232	−3.058	−4.543	−5.598	−5.733	−5.943	−8.089	0.351
0.600.....	−0.098	−0.458	−1.300	−2.142	−2.948	−4.387	−5.414	−5.550	−5.751	−8.109	0.417
0.700.....	−0.022	−0.489	−1.411	−2.212	−2.967	−4.341	−5.330	−5.466	−5.660	−8.147	0.539
0.800.....	0.346	−0.136	−1.227	−2.004	−2.707	−3.904	−4.794	−4.910	−5.089	−7.888	0.595
0.900.....	0.411	−0.123	−1.386	−2.200	−2.915	−4.134	−5.046	−5.169	−5.346	−7.838	0.662
1.000.....	0.566	0.050	−1.217	−2.004	−2.689	−3.825	−4.682	−4.795	−4.965	−7.755	0.677
1.500.....	0.843	0.099	−1.334	−2.148	−2.830	−3.926	−4.750	−4.858	−5.017	−7.502	0.761
2.000.....	1.049	0.343	−1.061	−1.866	−2.544	−3.646	−4.478	−4.588	−4.749	−7.232	0.752
3.000.....	1.137	0.395	−1.000	−1.802	−2.473	−3.538	−4.344	−4.444	−4.597	−6.945	0.774
4.000.....	1.168	0.334	−1.077	−1.882	−2.555	−3.641	−4.452	−4.554	−4.708	−6.764	0.813
5.000.....	1.206	0.353	−1.033	−1.823	−2.485	−3.534	−4.325	−4.421	−4.569	−6.592	0.833
					$Z = 0.001$, $Y = 0.246$						
0.025.....	−4.390	−3.844	−3.744	−3.844	−4.052	−4.739	−5.542	−5.669	−5.874	−9.366	−0.048
0.030.....	−4.128	−3.686	−3.599	−3.727	−4.001	−4.854	−5.764	−5.898	−6.114	−9.302	−0.014
0.050.....	−3.424	−3.079	−3.433	−4.176	−5.036	−6.762	−7.822	−7.979	−8.178	−9.186	0.267
0.080.....	−2.713	−2.484	−2.876	−3.599	−4.436	−6.154	−7.271	−7.438	−7.653	−8.987	0.269
0.100.....	−2.370	−2.182	−2.639	−3.400	−4.249	−5.973	−7.092	−7.261	−7.475	−8.894	0.299
0.200.....	−1.386	−1.469	−2.014	−2.815	−3.672	−5.429	−6.574	−6.747	−6.966	−8.574	0.366
0.300.....	−0.555	−0.943	−1.664	−2.500	−3.359	−5.116	−6.268	−6.440	−6.656	−8.364	0.410
0.400.....	−0.010	−0.486	−1.320	−2.131	−2.959	−4.694	−5.863	−6.039	−6.259	−8.191	0.432
0.500.....	0.319	−0.081	−1.062	−1.896	−2.720	−4.437	−5.603	−5.776	−5.997	−8.090	0.461
0.600.....	0.546	0.199	−0.933	−1.754	−2.533	−4.128	−5.240	−5.407	−5.621	−8.070	0.543
0.700.....	0.722	0.192	−1.172	−2.002	−2.742	−4.188	−5.226	−5.388	−5.583	−8.140	0.684
0.800.....	1.057	0.272	−1.255	−2.115	−2.860	−4.306	−5.321	−5.480	−5.668	−7.895	0.732
0.900.....	1.197	0.367	−1.170	−2.026	−2.763	−4.157	−5.147	−5.302	−5.487	−7.780	0.730
1.000.....	1.276	0.432	−1.101	−1.953	−2.681	−3.995	−4.929	−5.070	−5.248	−7.710	0.734
1.500.....	1.496	0.525	−1.038	−1.897	−2.625	−3.941	−4.865	−5.004	−5.181	−7.475	0.769
2.000.....	1.674	0.675	−0.890	−1.752	−2.479	−3.778	−4.686	−4.820	−4.994	−7.267	0.785
3.000.....	1.787	0.731	−0.813	−1.672	−2.399	−3.746	−4.674	−4.812	−4.989	−6.925	0.817
4.000.....	1.876	0.766	−0.769	−1.625	−2.353	−3.743	−4.696	−4.838	−5.017	−6.676	0.845
5.000.....	1.971	0.861	−0.655	−1.505	−2.230	−3.634	−4.594	−4.736	−4.916	−6.472	0.863
					$Z = 0.004$, $Y = 0.251$						
0.025.....	−4.851	−4.708	−4.679	−4.840	−5.147	−5.962	−6.738	−6.865	−7.036	−10.077	0.206
0.030.....	−4.219	−4.134	−4.193	−4.482	−4.931	−5.839	−6.566	−6.678	−6.829	−9.854	0.342
0.050.....	−3.323	−3.402	−3.550	−3.974	−4.659	−6.273	−7.415	−7.637	−7.875	−9.562	0.427
0.080.....	−2.071	−2.482	−2.817	−3.308	−4.052	−5.784	−6.999	−7.249	−7.509	−9.238	0.462
0.100.....	−1.397	−1.835	−2.412	−3.013	−3.821	−5.615	−6.850	−7.103	−7.366	−9.059	0.503
0.200.....	0.007	−0.109	−1.234	−2.129	−3.150	−5.163	−6.459	−6.723	−6.990	−8.525	0.553
0.300.....	0.487	0.355	−0.802	−1.711	−2.746	−4.817	−6.161	−6.439	−6.718	−8.287	0.537
0.400.....	1.070	0.853	−0.546	−1.605	−2.731	−4.818	−6.132	−6.388	−6.647	−8.070	0.561
0.500.....	1.436	1.175	−0.254	−1.335	−2.473	−4.592	−5.916	−6.180	−6.444	−7.918	0.574
0.600.....	1.708	1.303	−0.202	−1.277	−2.344	−4.276	−5.518	−5.744	−5.980	−7.835	0.598
0.700.....	1.807	1.096	−0.510	−1.516	−2.471	−4.190	−5.336	−5.547	−5.769	−7.895	0.695
0.800.....	1.852	0.971	−0.685	−1.679	−2.607	−4.270	−5.379	−5.585	−5.801	−7.952	0.763
0.900.....	2.027	1.066	−0.640	−1.658	−2.616	−4.348	−5.476	−5.690	−5.918	−7.665	0.764
1.000.....	2.120	1.127	−0.575	−1.587	−2.523	−4.187	−5.277	−5.476	−5.690	−7.569	0.760
1.500.....	2.477	1.291	−0.431	−1.441	−2.373	−4.032	−5.115	−5.310	−5.521	−7.273	0.802
2.000.....	2.615	1.320	−0.375	−1.370	−2.315	−4.021	−5.125	−5.328	−5.545	−7.122	0.866
3.000.....	2.789	1.441	−0.232	−1.228	−2.194	−3.929	−5.041	−5.244	−5.458	−6.775	0.918
4.000.....	2.900	1.478	−0.184	−1.174	−2.145	−3.886	−4.997	−5.198	−5.411	−6.497	0.945
5.000.....	2.977	1.583	−0.052	−1.042	−2.037	−3.829	−4.958	−5.163	−5.379	−6.279	0.962

TABLE 1—*Continued*

Age (Gyr) (1)	$\bar{M}_U$ (2)	$\bar{M}_B$ (3)	$\bar{M}_V$ (4)	$\bar{M}_R$ (5)	$\bar{M}_I$ (6)	$\bar{M}_J$ (7)	$\bar{M}_H$ (8)	$\bar{M}_K$ (9)	$\bar{M}_L$ (10)	$M_V^{\rm tot}$ (11)	$V-I$ (12)
					$Z = 0.008$, $Y = 0.256$						
0.025.....	−4.259	−4.523	−4.596	−4.841	−5.259	−6.121	−6.835	−6.963	−7.119	−10.214	0.445
0.050.....	−1.598	−1.556	−2.816	−3.630	−4.521	−5.892	−6.959	−7.236	−7.548	−9.402	0.674
0.080.....	−0.855	−0.641	−1.906	−2.839	−3.994	−5.634	−6.840	−7.144	−7.483	−9.058	0.643
0.100.....	−0.561	−0.386	−1.597	−2.532	−3.756	−5.483	−6.739	−7.051	−7.398	−8.912	0.610
0.200.....	0.126	0.193	−0.757	−1.681	−3.083	−5.012	−6.384	−6.722	−7.092	−8.497	0.539
0.300.....	0.843	0.814	−0.262	−1.331	−2.903	−4.886	−6.273	−6.605	−6.966	−8.221	0.560
0.400.....	1.332	1.209	0.110	−1.028	−2.658	−4.638	−6.027	−6.348	−6.701	−8.008	0.566
0.500.....	1.680	1.432	0.206	−0.985	−2.543	−4.433	−5.767	−6.058	−6.381	−7.873	0.600
0.600.....	1.962	1.578	0.203	−1.016	−2.548	−4.412	−5.728	−6.017	−6.338	−7.769	0.635
0.700.....	2.147	1.543	0.018	−1.141	−2.543	−4.307	−5.569	−5.850	−6.164	−7.773	0.722
0.800.....	2.273	1.426	−0.225	−1.338	−2.528	−4.096	−5.218	−5.448	−5.700	−7.806	0.796
0.900.....	2.377	1.486	−0.178	−1.297	−2.572	−4.221	−5.407	−5.673	−5.978	−7.522	0.803
1.000.....	2.491	1.553	−0.127	−1.253	−2.530	−4.170	−5.345	−5.603	−5.901	−7.443	0.822
1.500.....	2.903	1.721	0.016	−1.097	−2.411	−4.081	−5.276	−5.554	−5.870	−7.113	0.898
2.000.....	3.142	1.817	0.089	−1.034	−2.358	−3.970	−5.132	−5.382	−5.667	−6.895	0.953
3.000.....	3.357	1.962	0.276	−0.839	−2.232	−3.862	−5.043	−5.298	−5.594	−6.573	1.013
4.000.....	3.503	2.056	0.398	−0.712	−2.181	−3.871	−5.085	−5.363	−5.683	−6.317	1.050
5.000.....	3.659	2.197	0.554	−0.548	−2.048	−3.773	−5.010	−5.298	−5.630	−6.080	1.062
					$Z = 0.01$, $Y = 0.259$						
0.025.....	−4.220	−3.903	−3.978	−4.386	−4.994	−6.064	−6.851	−6.991	−7.149	−9.914	0.416
0.030.....	−3.775	−3.848	−3.987	−4.342	−4.877	−5.854	−6.618	−6.755	−6.911	−9.882	0.464
0.050.....	−1.542	−1.176	−2.485	−3.417	−4.403	−5.884	−6.969	−7.283	−7.602	−9.346	0.682
0.080.....	−0.910	−0.585	−1.755	−2.697	−3.884	−5.612	−6.823	−7.169	−7.515	−9.043	0.621
0.100.....	−0.627	−0.419	−1.534	−2.454	−3.709	−5.505	−6.760	−7.109	−7.457	−8.920	0.592
0.200.....	0.191	0.257	−0.680	−1.600	−3.040	−5.059	−6.432	−6.807	−7.177	−8.498	0.531
0.300.....	0.894	0.909	−0.010	−1.050	−2.703	−4.809	−6.207	−6.577	−6.944	−8.189	0.542
0.400.....	1.365	1.260	0.297	−0.838	−2.594	−4.660	−6.045	−6.395	−6.747	−7.975	0.558
0.500.....	1.708	1.446	0.187	−1.073	−2.722	−4.618	−5.919	−6.232	−6.550	−7.843	0.614
0.600.....	2.023	1.628	0.261	−1.007	−2.658	−4.545	−5.843	−6.158	−6.478	−7.744	0.653
0.700.....	2.222	1.567	0.015	−1.154	−2.567	−4.277	−5.490	−5.782	−6.082	−7.765	0.756
0.800.....	2.347	1.482	−0.167	−1.304	−2.624	−4.274	−5.448	−5.739	−6.039	−7.796	0.846
0.900.....	2.473	1.572	−0.117	−1.292	−2.665	−4.314	−5.475	−5.754	−6.047	−7.511	0.854
1.000.....	2.590	1.683	−0.002	−1.179	−2.566	−4.222	−5.390	−5.670	−5.964	−7.400	0.859
1.500.....	3.032	1.877	0.171	−0.974	−2.382	−4.085	−5.275	−5.578	−5.890	−7.037	0.927
2.000.....	3.317	1.998	0.273	−0.873	−2.319	−4.034	−5.226	−5.530	−5.843	−6.812	0.982
3.000.....	3.569	2.132	0.434	−0.698	−2.193	−3.943	−5.144	−5.452	−5.772	−6.504	1.046
4.000.....	3.688	2.241	0.580	−0.543	−2.072	−3.809	−5.013	−5.310	−5.623	−6.240	1.077
5.000.....	3.798	2.284	0.637	−0.474	−2.022	−3.826	−5.047	−5.366	−5.695	−6.035	1.103
					$Z = 0.0198$, $Y = 0.273$						
0.025.....	−4.341	−4.161	−4.143	−4.356	−4.902	−5.894	−6.777	−6.961	−7.123	−10.042	0.318
0.050.....	−2.683	−2.920	−3.080	−3.409	−4.134	−5.968	−7.145	−7.626	−7.970	−9.545	0.417
0.080.....	−1.435	−1.423	−2.031	−2.609	−3.571	−5.775	−7.021	−7.521	−7.871	−9.172	0.458
0.100.....	−0.887	−0.696	−1.442	−2.175	−3.291	−5.655	−6.925	−7.441	−7.800	−8.979	0.492
0.200.....	0.237	0.388	−0.171	−1.024	−2.530	−5.271	−6.587	−7.098	−7.456	−8.433	0.488
0.300.....	0.937	0.911	0.291	−0.669	−2.396	−5.087	−6.387	−6.859	−7.192	−8.134	0.533
0.400.....	1.418	1.270	0.500	−0.567	−2.432	−4.957	−6.232	−6.681	−7.000	−7.915	0.587
0.500.....	1.826	1.585	0.692	−0.435	−2.326	−4.719	−5.983	−6.419	−6.731	−7.754	0.632
0.600.....	2.136	1.778	0.680	−0.490	−2.334	−4.656	−5.899	−6.330	−6.639	−7.644	0.689
0.700.....	2.435	1.890	0.487	−0.700	−2.309	−4.380	−5.564	−5.976	−6.273	−7.628	0.813
0.800.....	2.619	1.939	0.444	−0.739	−2.333	−4.350	−5.519	−5.933	−6.230	−7.594	0.883
0.900.....	2.739	1.997	0.422	−0.792	−2.432	−4.526	−5.673	−6.086	−6.379	−7.358	0.944
1.000.....	2.869	2.075	0.453	−0.761	−2.381	−4.429	−5.575	−5.984	−6.276	−7.225	0.949
1.500.....	3.382	2.385	0.702	−0.497	−2.131	−4.243	−5.391	−5.791	−6.076	−6.817	1.007
2.000.....	3.770	2.547	0.838	−0.335	−1.930	−4.077	−5.231	−5.639	−5.927	−6.574	1.049
3.000.....	4.109	2.686	0.971	−0.204	−1.849	−4.135	−5.289	−5.713	−6.010	−6.256	1.101
4.000.....	4.250	2.722	1.049	−0.079	−1.651	−4.029	−5.187	−5.632	−5.939	−6.024	1.137
5.000.....	4.396	2.840	1.177	0.051	−1.548	−4.040	−5.192	−5.639	−5.943	−5.817	1.174

TABLE 1—*Continued*

Age (Gyr) (1)	$\bar{M}_U$ (2)	$\bar{M}_B$ (3)	$\bar{M}_V$ (4)	$\bar{M}_R$ (5)	$\bar{M}_I$ (6)	$\bar{M}_J$ (7)	$\bar{M}_H$ (8)	$\bar{M}_K$ (9)	$\bar{M}_L$ (10)	$M_V^{\rm tot}$ (11)	$V-I$ (12)
						$Z = 0.04,\ Y = 0.30$					
0.025.....	−3.985	−4.192	−4.247	−4.393	−4.800	−5.750	−6.630	−6.870	−7.058	−10.056	0.305
0.030.....	−3.390	−3.752	−3.931	−4.142	−4.664	−6.723	−7.857	−8.348	−8.671	−9.936	0.374
0.050.....	−1.901	−1.692	−2.450	−3.089	−3.875	−6.023	−7.214	−7.785	−8.173	−9.413	0.490
0.080.....	−1.166	−0.690	−1.206	−1.999	−3.076	−5.728	−6.952	−7.529	−7.915	−8.996	0.498
0.100.....	−0.828	−0.401	−0.796	−1.548	−2.698	−5.627	−6.890	−7.489	−7.884	−8.831	0.479
0.200.....	0.259	0.368	0.099	−0.580	−1.934	−5.302	−6.621	−7.230	−7.628	−8.329	0.474
0.300.....	0.954	0.914	0.560	−0.170	−1.602	−5.143	−6.456	−7.048	−7.431	−8.015	0.533
0.400.....	1.549	1.363	0.840	0.043	−1.590	−5.037	−6.322	−6.878	−7.243	−7.785	0.596
0.500.....	1.972	1.717	1.030	0.147	−1.616	−4.866	−6.127	−6.661	−7.016	−7.607	0.653
0.600.....	2.319	2.016	1.147	0.201	−1.576	−4.726	−5.974	−6.501	−6.850	−7.461	0.709
0.700.....	2.594	2.249	1.156	0.100	−1.801	−4.996	−6.188	−6.693	−7.026	−7.328	0.807
0.800.....	2.727	2.400	1.188	0.030	−1.607	−4.557	−5.768	−6.285	−6.625	−6.919	0.775
0.900.....	2.915	2.556	1.232	0.020	−1.698	−4.488	−5.674	−6.171	−6.498	−6.811	0.833
1.000.....	3.104	2.646	1.225	−0.001	−1.744	−4.505	−5.676	−6.166	−6.492	−6.718	0.878
1.500.....	3.695	2.746	1.158	0.030	−1.572	−4.316	−5.463	−5.956	−6.282	−6.585	1.044
2.000.....	4.063	2.851	1.232	0.120	−1.467	−4.218	−5.358	−5.845	−6.163	−6.334	1.089
3.000.....	4.466	3.051	1.422	0.330	−1.224	−4.136	−5.286	−5.795	−6.123	−5.992	1.135
4.000.....	4.662	3.166	1.546	0.461	−1.094	−4.078	−5.230	−5.744	−6.077	−5.761	1.158
5.000.....	4.796	3.245	1.633	0.558	−0.979	−3.999	−5.152	−5.674	−6.012	−5.590	1.183

appearance of AGB stars is expected to produce a less intense variation in the NIR SBF of a metal-rich population.

Looking at both Figures 3 and 5, one can note that the strong dependence of the NIR SBF on mass loss, especially for intermediate-age populations, has several implications. The NIR SBF with intermediate mass loss (B1 model) can look similar to those with mild mass loss (BH model), depending on metallicity. This behavior might generate a possible problem of degeneracy when the metallicity of the stellar system is unknown. In addition, the evidence that mass loss increases with metallicity in AGB stars (Groenewegen et al. 1995) might complicate the scenario. On the other hand, this high sensitivity can be used to discriminate among different mass loss assumptions, if stellar systems with known metallicity are considered, thus making SBFs an interesting tool for investigating properties of AGB stars. In § 4 we use *HST* WFPC2 SBF data to discriminate the mass-loss scenario active in the TP-AGB stars for a sample of LMC star clusters.

4. SBF MEASUREMENTS

To our knowledge, optical-SBF models available in the literature do not include predictions for young stellar populations, as they usually extend down to 2–5 Gyr (Worthey 1993; Buzzoni 1993; Liu et al. 2000; Blakeslee et al. 2001; Paper I). Thus, no comparison with optical SBF models from other authors can be done. In this section we provide the first step toward the measure of optical SBFs for young SSPs.

Stellar clusters in the Magellanic Clouds (MCs) represent a unique opportunity to explore the behavior of SBFs in young and intermediate-age stellar systems. The MC clusters—formed at different epochs—provide a remarkable sampling of stellar clusters in a wide range of ages. Moreover, because of their proximity, they allow us to perform direct photometry of individual stars. This is of paramount importance in probing stellar population synthesis tools and models. The criteria for selecting MC star clusters, as well as photometric data analysis, are two important steps in our overall investigation. Hence, in § 4.1 we describe these steps in detail before discussing the SBF measurements.

4.1. *Star Clusters and Photometric Data Selection*

As shown in § 3.1, the low statistic in the brighter part of the cluster LF plays a role in determining the uncertainties of the measured SBFs. For this reason we prefer clusters with a number of stars high enough to avoid large statistical fluctuations (Fig. 2). While taking this condition into account, we give the priority to more massive clusters by selecting young LMC clusters, whose integrated magnitudes satisfy the condition $M_V^{\rm tot} \lesssim M_V^{\rm tot,\,max}$ at any age.

An accurate photometry of individual stars in the cluster core is another crucial requirement in order to fully map all the features of the cluster stellar population. We take advantage of the *HST* WFPC2 high capability of resolving stars in the core of the MC clusters. Mackey & Gilmore (2003, hereafter MG03) have shown that the core radius of MC clusters is typically smaller than 30″; thus, the WFPC2 field of view is large enough to contain most stars in the cluster.

With a total apparent magnitude $V^{\rm tot} = 9.89 \pm 0.01$ (van den Bergh 1981), NGC 1866 is one of the most massive clusters formed in the LMC during the last 3 Gyr. Our group has recently obtained deep and accurate *HST* WFPC2 observations in the F555W ($\sim V$) and F814W ($\sim I$) filters of this cluster (Walker et al. 2001; Brocato et al. 2003). Hence, it is a good candidate for our purpose. Further, we select a sample of LMC clusters spanning the age range from a few million up to a few billion years, for which similar *HST* observations in the same photometric filters are available. A subsample of the LMC clusters studied by de Grijs et al. (2002a, 2002b, 2002c) satisfies most requirements, namely, NGC 1805, NGC 1818, NGC 1831, NGC 1868, NGC 2209, and Hodge 14. Their observations, just like our own for NGC 1866, reach magnitudes as faint as $V \sim 25$ mag. Moreover, de Grijs and collaborators could detect radial mass segregation in the central regions of these LMC clusters. This is a clear indication of the high level of completeness and accuracy of their photometric data and LFs.

In order to minimize possible differences in handling the data, the original images have been retrieved from the *HST* archive and

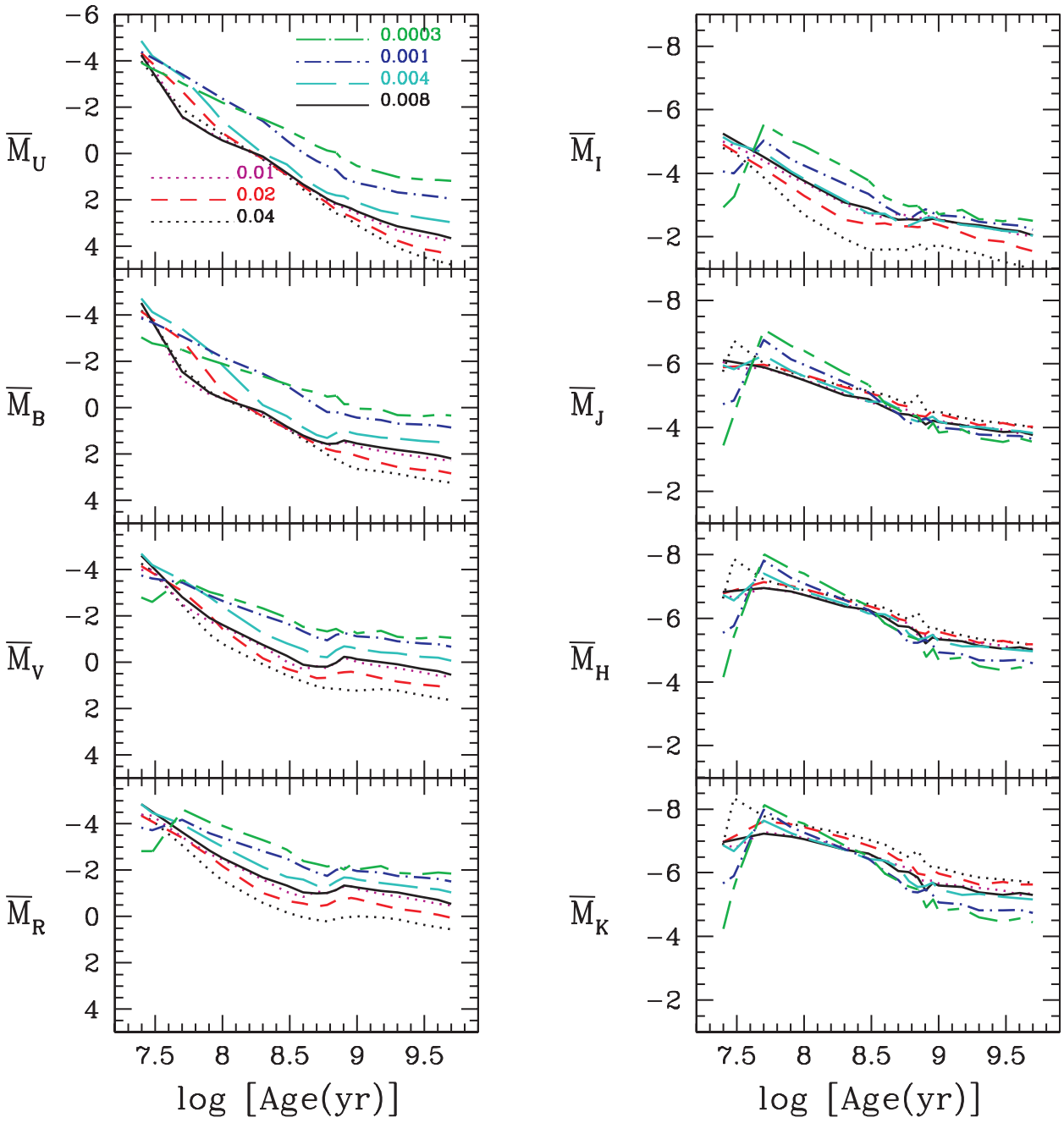

FIG. 5.—Time evolution of SBF magnitudes for different metallicities (B1 models). The different lines represent the labeled metallicity values.

analyzed by following the same procedure as discussed in Brocato et al. (2003), briefly described here. The basic information on the images we used is summarized in Table 2. Each frame has been preprocessed according to the standard WFPC2 pipeline, using the latest available calibrations. The removal of cosmic rays and the photometry were performed with the most recent version of the HSTphot package developed by Dolphin (2000a). The point-spread function (PSF)–fitting option in the HSTphot routine was adopted in order to take advantage of the PSFs, which are computed directly to reproduce the shape details of star images as obtained in the different regions of the WFPC2. Charge transfer efficiency corrections and calibrations to the standard *VI* system were obtained directly by HSTphot routines, as documented by Dolphin (2000b). In Figure 6 the resulting CMDs are plotted, together with the typical uncertainties of the photometry as a function of magnitude. The V and I photometry of de Grijs and collaborators is compared with the present work. The agreement is extremely good, with mean differences on the order of a few hundreds of magnitudes in all the chips and for all the clusters. Completeness was evaluated by distributing artificial stars of known positions and magnitudes in selected circular regions around the cluster center. Since the resulting completeness functions strictly agree with those published by de Grijs et al. (2002b, 2002c; see their Fig. 2), we do not present our nearly identical figures.

Even though the present paper is mainly devoted to young stellar clusters, for the sake of completeness we also added four really old clusters. We derived $\bar{V}$ and $\bar{I}$ also for NGC 1754, 1916, 2005, and 2019 by relying on the high-quality, deep *HST* photometry by Olsen et al. (1998), who used deep exposures in both

TABLE 2
OVERVIEW OF THE WFPC2 OBSERVATIONS FOR YOUNG CLUSTERS IN THE SAMPLE

Cluster	Archive Directory/File	Filter	Total Exposure Time (s)	Date
NGC 1805.....	u4ax0204b	F555W	435	1998 Jul 25
	u4ax020ab	F814W	960	1998 Jul 25
	u4ax0501b	F555W	7200	1998 Mar 12
	u4ax0601b	F814W	4800	1998 Mar 12
	u4ax0803b	F555W	2500	1998 Apr 29
	u4ax0903b	F814W	2500	1998 Apr 28
NGC 1818.....	u4ax3004b	F555W	435	1998 Sep 25
	u4ax300ab	F814W	960	1998 Sep 25
	u4ax3301b	F555W	7200	1998 Jul 11
	u4ax3501b	F814W	4800	1998 Jul 29
	u4ax3603b	F555W	2500	1998 Apr 30
	u4ax3703b	F814W	2500	1998 Apr 30
NGC 1868.....	u4ax5204b	F555W	435	1998 Nov 12
	u4ax520ab	F814W	960	1998 Nov 12
	u4ax5301b	F555W	7200	1998 Mar 21
	u4ax5601b	F814W	4800	1998 Mar 22
	u4ax5803b	F555W	2500	1998 May 20
	u4ax5903b	F814W	2500	1998 May 24
NGC 1831.....	u4ax4104b	F555W	435	1998 Jul 25
	u4ax410ab	F814W	960	1998 Jul 25
	u4ax4401b	F555W	7200	1998 Jul 24
	u4ax4601b	F814W	4800	1998 Jul 24
	u4ax4703b	F555W	2500	1998 May 29
	u4ax4803b	F814W	2500	1998 May 30
NGC 2209.....	u4ax6304b	F555W	435	1998 Mar 29
	u4ax630ab	F814W	960	1998 Mar 29
	u4ax6401b	F555W	7200	1998 Mar 28
	u4ax6701b	F814W	4800	1998 Apr 3
	u4ax6903b	F555W	2500	1998 May 6
	u4ax7003b	F814W	2500	1998 May 5
Hodge 14.....	u4ax7404b	F555W	435	1998 Mar 31
	u4ax740ab	F814W	960	1998 Mar 31
	u4ax7301b	F555W	1200	1998 Feb 4
	u4ax7303b	F814W	800	1998 Feb 4
	u4ax7501b	F555W	7200	1998 Aug 6
	u4ax7801b	F814W	4800	1998 Aug 5

the F555W and F814W filters. This assures the measurement of stars of $V \sim 25$, well below the main-sequence turnoff (MSTO) point for all the clusters.

Finally, we have a sample of 11 LMC star clusters. The complete list and a few properties of the clusters are presented in Table 3: cluster name (col. [1]); total V magnitude from van den Bergh (1981) and the present work (cols. [2] and [3]); $\bar{V}$, $\bar{I}$, and $\bar{V} - \bar{I}$ (cols. [4]–[6]); and cluster age as derived in § 4.3 (col. [7]) or from the literature (col. [8]). The uncertainties of SBF data refer to the maximum/minimum SBF values obtained by including field contamination and "missed" bright stars, as described in § 4.2. The integrated magnitudes obtained in the present work refer to the photometric data used to derive the SBF measurements. They agree with the values of van den Bergh (1981) within a few tenths of magnitudes. For Hodge 14 the difference is larger due to the severe area selection we used in order to minimize the field contamination (see § 4.2).

4.2. *Optical SBF*

In order to measure SBFs, we followed the procedure described by AT94, which uses the photometry of individual stars in the cluster. Stars 8–10 mag fainter than the brightest stars of the cluster were measured through high-resolution WFPC2 imaging. This allowed us to use individual-star photometry not only to evaluate the numerator in equation (4) but also the denominator without introducing other sources of uncertainty in estimating the total flux (e.g., sky-level evaluation). Differently from the present work, AT94 (and G04) were forced "to sum the flux of the CCD image with the sky subtracted" to account for the contribution of the large number of unmeasured faint stars to the total flux. This is due to the fact that the photometry used in those papers does not reach the faint part of the MS (see, e.g., the case of 47 Tuc in Fig. 10 of AT94).

The faint magnitude limit of the photometry is a crucial point in evaluating the denominator of equation (4), as demonstrated by AT94. In order to find a quantitative indication of the impact of faint MS stars on SBFs, we used the following procedure: First, the *VI* SBFs are derived from synthetic *VI* CMDs, containing stars with masses down to $m = 0.1\ M_{\odot}$, by applying the RS procedure (eq. [4]). Then, the SBFs are recomputed by artificially cutting out stars with $V > V_{\rm cut}$ from the complete synthetic CMDs for a selected set of $V_{\rm cut}$. This test corresponds to a simulation of 100% incompleteness at magnitudes fainter than $V_{\rm cut}$. The *V*- and *I*-band SBFs were derived by adopting the LMC absolute distance modulus $(m - M)_0 = 18.4 \pm 0.1$ and mean reddening $E_{B-V} = 0.06$ (Walker et al. 2001; Alcock et al. 2004). The procedure was repeated for three different populations, aged $t = 100$ Myr, 900 Myr, and 4 Gyr. The differences between the SBFs derived by considering the complete synthetic CMDs and those from the "cut" ones are presented in Figure 7 as a function of $V_{\rm cut}$. The figure shows that the younger the cluster, the brighter the completeness limit required to minimize the difference between SBFs computed by including all stars of the CMD and SBFs obtained by including only stars with $V < V_{\rm cut}$. For clusters as old as $t = 4$ Gyr, the uncertainty of SBFs introduced by incompleteness is $\leq$0.2 mag in $\bar{V}$ and $\leq$0.03 mag in $(\bar{V} - \bar{I})$ if $V_{\rm cut} \geq 23$ mag. For clusters younger than $\sim$900 Myr, the uncertainty of the SBFs keeps below 0.2 mag in $\bar{V}$ and $\lesssim$0.05 mag in $(\bar{V} - \bar{I})$ if $V_{\rm cut} \geq 21$ mag.

As regards the LMC clusters considered here, the completeness of NGC 2209 and Hodge 14 is shown to be larger than 90% for V and $I \leq 23$, while for younger clusters (NGC 1805, 1818, 1831, 1866, and 1868), it is larger than $\sim$80%–90% for V and $I \lesssim 21$ except for the innermost annulus, i.e., $r \leq 3\farcs6$ (de Grijs et al. 2002b, 2002c; Brocato et al. 2003). As for old clusters (NGC 1754, 1916, 2005, and 2019), we used the photometric data by Olsen et al. (1998), who made deep exposures in both the F555W and F814W filters. This allowed us to reach $V \sim 25$ mag, well below the MSTO point. Again, for all these clusters, completeness at $V \leq 23$ mag is assured to be more than 80% for $r \geq 5''$.

Thus, the uncertainty of $\bar{V}$ and $\bar{I}$ due to the incompleteness is very small, well below 0.2 mag for all the ages considered. This ensures that $\bar{V}$ and $\bar{I}$ are derived with a degree of precision adequate for the level of intrinsic uncertainty due to statistical fluctuations expected for LMC clusters (§ 3.1).

Crowding effects might also be relevant in evaluating the numerator of equation (4). The technique of distributing artificial stars also helps in studying this issue. From Figure 2 by de Grijs et al. (2002b), it is evident that NGC 1831, NGC 1868, NGC 2209, and Hodge 14 are not affected by crowding effects, showing $\sim$100% completeness for the brightest 3 mag of the cluster stars. Similar evidence can be derived for NGC 1866 (Brocato et al. 2003). On the other hand, NGC 1805 and NGC 1818 may suffer 10% missed stars within $7\farcs2$ of the center (representing less than 3.5% of the Planetary Camera [PC] area). Since the completeness functions have a statistical meaning, a single young

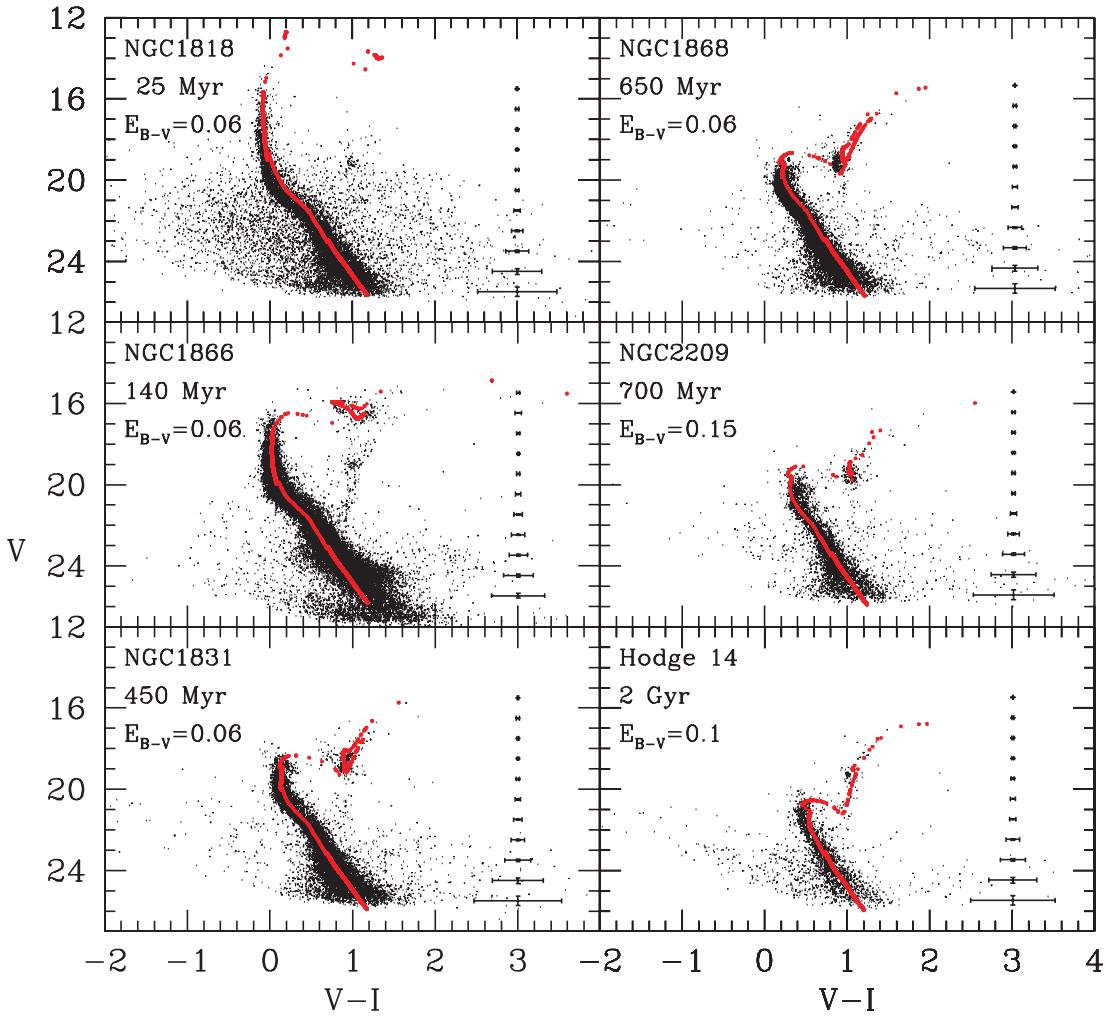

FIG. 6.—Comparison of observed (*black dots*) and synthetic (*red dots*) CMDs of a sample of LMC clusters. In each panel the best fit is plotted, together with the derived reddening value. We adopt $Z = 0.008$ and an absolute distance modulus of $(m - M_V)_0 = 18.4$. Photometric errors are also indicated on the right side of each panel.

cluster has been further analyzed in order to check whether very bright stars are missed due to crowding effects and/or saturation problems. For clusters younger than a few billion years, we must pay particular attention to bright and cool AGB stars, which may strongly affect the SBF measurements. In order to check the completeness of the brightest end of the LF, we retrieved for each cluster the images and the JHK_s photometry available in the final release of the Two Micron All Sky Survey (2MASS).[7] Then, a star-by-star cross-identification between the two sets of photometry (*HST* and 2MASS) was performed to avoid missing cool

[7] See http://www.ipac.caltech.edu/2mass.

TABLE 3
CLUSTER PROPERTIES AND MEASURED SBFS

Source (1)	V_{tot}[a] (2)	V_{tot} (3)	$\bar{V}$ (4)	$\bar{I}$ (5)	$\bar{V} - \bar{I}$ (6)	log [t(yr)] (7)	References[b] (8)
NGC 1805	10.63	10.9	15.31 ± 0.2	15.30 ± 0.2	0.01 ± 0.3	$7.00^{+0.30}_{-0.10}$	1
NGC 1818	9.70	10.2	15.00 ± 1.0	14.37 ± 1.0	0.63 ± 1.0	7.40 ± 0.30	2
NGC 1866	9.73	9.4	17.09 ± 0.2	14.95 ± 0.2	2.14 ± 0.07	8.15 ± 0.30	3
NGC 1831	11.18	10.9	18.47 ± 0.2	15.90 ± 0.2	2.57 ± 0.3	8.65 ± 0.30	2
NGC 1868	11.56	11.5	18.68 ± 0.5	16.50 ± 0.5	2.18 ± 0.5	8.81 ± 0.30	2
NGC 2209	13.15	12.5	18.75 ± 0.5	16.66 ± 0.5	2.09 ± 0.5	8.85 ± 0.20	2
Hodge 14	11.45	13.7	19.21 ± 1.0	17.29 ± 1.0	1.92 ± 0.5	9.30 ± 0.10	2
NGC 1754	11.86	12.2	18.42 ± 0.5	16.70 ± 0.5	1.72 ± 0.4	$10.19^{+0.06}_{-0.07}$	1
NGC 1916	10.38	10.9	18.10 ± 0.5	16.28 ± 0.5	1.83 ± 0.4	10.20 ± 0.09	1
NGC 2005	11.57	11.7	18.18 ± 0.5	16.11 ± 0.5	2.07 ± 0.4	$10.22^{+0.12}_{-0.16}$	1
NGC 2019	10.86	11.4	17.94 ± 0.5	16.13 ± 0.5	1.81 ± 0.4	$10.25^{+0.07}_{-0.09}$	1

[a] Van den Bergh (1981).
[b] References for the cluster age: (1) MG03; (2) this work; (3) Brocato et al. (2003).

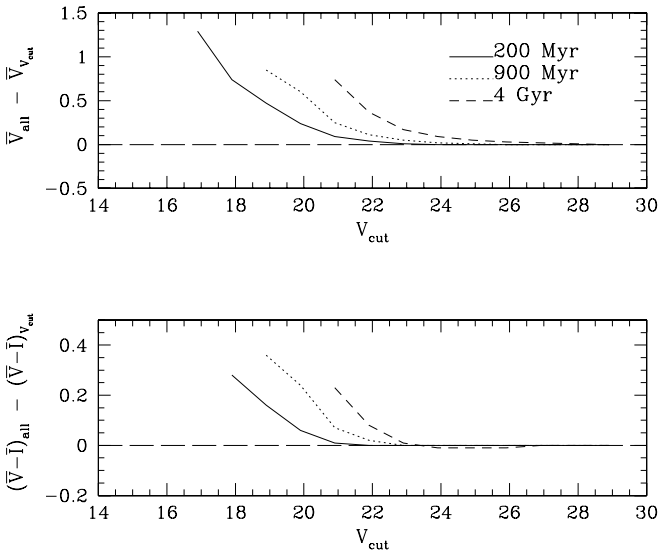

FIG. 7.—Impact of the completeness limit V_{cut} on SBFs. The differences are between SBFs obtained using a synthetic CMD complete down to star mass $m = 0.1\ M_{\odot}$ and SBFs from the same CMD but excluding stars with $V > V_{cut}$ (i.e., 100% incompleteness at $V > V_{cut}$). The labeled ages and a fixed metallicity $Z = 0.008$ are adopted.

AGB stars within the observed field for the final photometric list used to derive SBFs. If we missed one or more cool stars in the *HST* photometry, their corresponding V and I magnitudes were obtained from the literature. The V and I magnitudes of such bright and cool AGB stars are available in the literature mainly because of the large efforts in the past in searching for AGB carbon-rich stars (C-stars) in the LMC clusters (e.g., Aaronson & Mould 1982; Westerlund et al. 1991).

However, there is no guarantee that such bright stars found within the observed cluster field all belong to the cluster. For this reason we provide—as an indicative uncertainty of the SBF measurements—half the difference between the SBF computed using only stars within the PC field and the SBF obtained by adding to the photometric list the *missed* bright stars. This is a safe assumption, which probably leads to an overestimate of the uncertainty. Nevertheless, the primary goal of this paper is to explore the general behavior of optical SBFs of young stellar populations, leaving a detailed and quantitative analysis of LMC clusters to a forthcoming paper.

In the data analysis we also looked for another severe effect of crowding, the blending effect. The completeness curves we considered are corrected for it, as well as for superposition of multiple randomly placed artificial stars. However, to make a further check, we estimated the number of expected blended pairs as discussed by Stephens et al. (2001). Dealing with *HST* WFPC2, even in the worst case of a very densely populated core of a cluster such as NGC 1866, the number of blended pairs formed by two identical giant stars is estimated to be on the order of 0.0001% for the PC and about 0.01% for the wide-field chips.

The field star contamination is not severe for the selected clusters (with the exception of Hodge 14). The contribution of field stars to SBF measurements is evaluated by comparing SBF magnitudes derived from the whole region covered by the WFPC2 with the results obtained from the PC area only, which typically includes most of the stars of the cluster.

Finally, the four truly old clusters show SBF magnitudes in very good agreement with the average SBF values obtained for the GGCs by AT94. This last point can also be seen as a posteriori verification that our method of measuring SBFs from high-quality, deep photometric data is reliable, at least for the purpose of the present paper.

4.3. *Age Determination*

We used current synthetic CMDs to consistently evaluate the age of each cluster. In Figure 6 we show the comparison between the observed CMDs and the synthetic ones. For all the clusters we assumed a metallicity equal to $Z = 0.008$ and an absolute distance modulus of $(m - M)_0 = 18.4 \pm 0.1$. The reddening value of each cluster was derived from the best-fitting procedure as discussed in Walker et al. (2001). The assumed distance to the LMC appears justified in light of recent distance measurements, which attempt to reconcile the long- with the short-distance scale (e.g., Salaris et al. 2003; Alcock et al. 2004).

The cluster age and the related overall uncertainty are reported in Table 3 (col. [7]). They are in good agreement with ages listed by MG03. The interstellar reddening values fall within the range measured for the LMC, e.g., $E_{B-V} = 0.06$–0.20 (Westerlund 1997).

Figure 6 confirms the extremely high degree of accuracy that our SSP models reach in simulating the CMDs of young stellar populations. In addition, we remark that our procedure is fully consistent, since the same theoretical framework was adopted for computing SBFs and for the CMD analysis aimed at obtaining the age of each cluster.

5. MODELS VERSUS OBSERVATIONS

5.1. *Optical SBFs*

In this section we compare SBF predictions with the optical measurements. As discussed in § 3.2, the $(\bar{V} - \bar{I})$ fluctuation color is sensitive to the mass-loss rate in the final stages of the AGB. In Figure 8 observational data for clusters with age

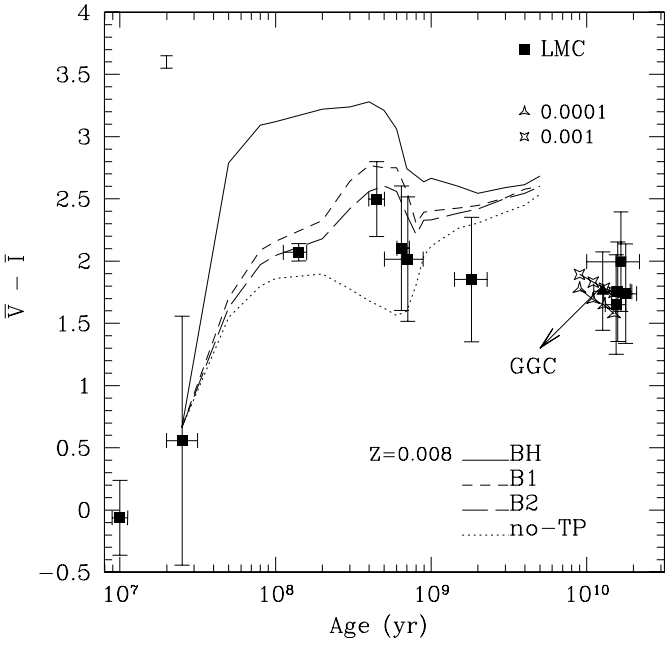

FIG. 8.—$(\bar{V} - \bar{I})$ fluctuation color vs. age. For ages lower than 5 Gyr, models with $Z = 0.008$ and different mass-loss rates are plotted (symbols are as in Fig. 3). For ages larger than 5 Gyr, models with $Z = 0.0001$ (*three-pointed stars*) and $Z = 0.001$ (*four-pointed stars*) are from Paper I. The LMC star cluster fluctuation colors are shown as black filled squares. The triangle refers to the mean $(\bar{V} - \bar{I})$ color of GGCs (data from AT94). At the upper left we show the mean error bar of the SBF models. [*See the electronic edition of the Journal for a color version of this figure.*]

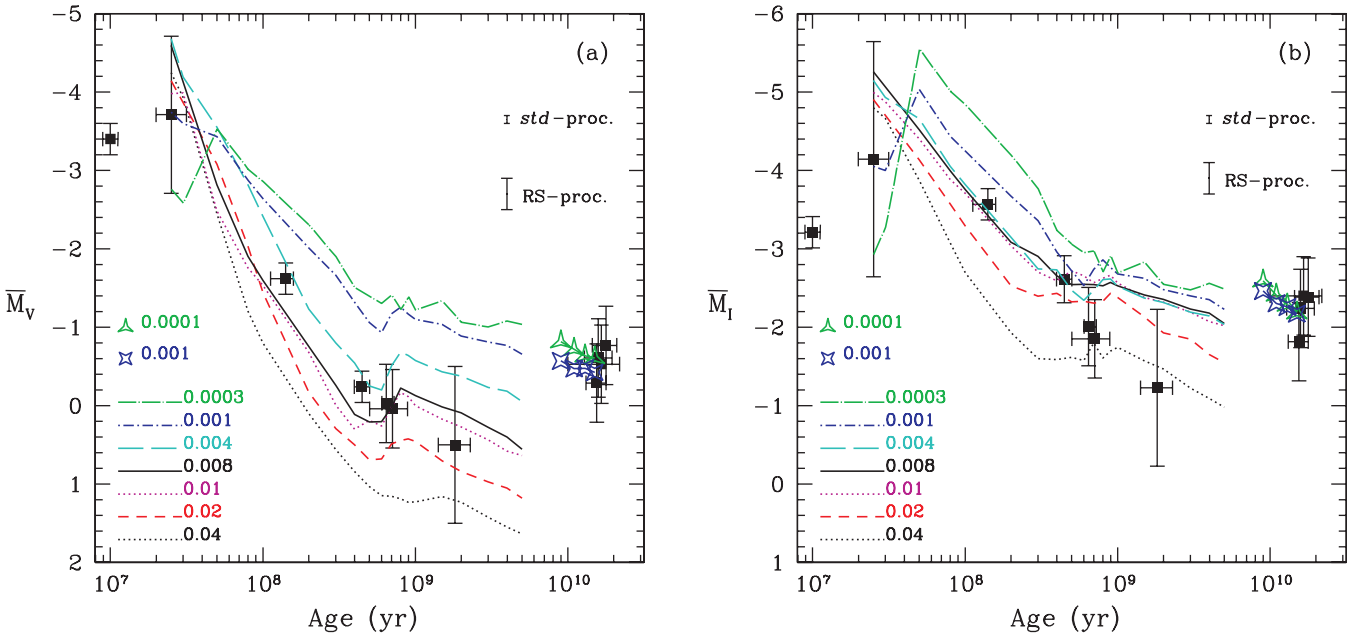

FIG. 9.—(*a*) $\bar{M}_V$ and (*b*) $\bar{M}_I$ as a function of age. For ages lower than 5 Gyr, only models with the B1 mass-loss rate are considered. Models for $t > 5$ Gyr are from Paper I (symbols as in Fig. 8). Black filled squares refer to the measured SBF amplitudes for LMC star clusters. The expected theoretical uncertainties are shown in the upper right corner of each panel (see text).

$t < 5$ Gyr are located within the two theoretical curves representing models *without* TP-AGB stars (no-TP, *dotted line*) and models computed by assuming the BH83 mass-loss rate (*solid line*). The cluster Hodge 14 is the only exception: we discuss it below. Being the least efficient rate explored in the present work, the BH83 mass-loss rate predicts a large number of TP stars, which are responsible for very "red" ($\bar{V} - \bar{I}$) colors of young SSPs. In spite of the large error bars of the LMC cluster data, Figure 8 suggests that the B1 and B2 models give a better fit than the BH models for nearly all the clusters. In particular, NGC 1866, for which we succeed in minimizing the uncertainties, is well fitted by models with mass-loss prescriptions by B95.

In the same figure, old and very metal-poor models ($t > 5$ Gyr, $Z = 0.001$ and 0.0001) published in Paper I are plotted as three- and four-pointed stars. They were computed assuming a Reimers mass-loss rate (see Paper I for details). Note that models of age $t > 5$ Gyr fully consistent with the present theoretical scenario will be discussed in a forthcoming paper (see footnote 5).

Figure 9 exhibits the $\bar{M}_V$ and $\bar{M}_I$ behavior with age. For $t <$ 5 Gyr we plot SBF models of all the metallicities given in the present paper; only the B1 mass-loss scenario is used. For older clusters, models with $Z = 0.001$ and 0.0001 are taken from Paper I. The theoretical SBFs refer to the asymptotic values (standard procedure) for which the uncertainty is on the order of 0.05 mag, as already discussed. We also evaluated the *intrinsic* uncertainty due to stochastic effects on the number of bright stars (RS procedure) from the models with the faintest $M_V^{\rm tot}$ (Table 1). According to the discussion in § 3.1, the fainter the integrated V magnitude of the cluster, the larger the *intrinsic* uncertainty. We finally find out that it is on the order of 0.2 mag.

The general trend of $\bar{M}_V$ for LMC clusters is well reproduced by models in the explored age range (Fig. 9*a*). The SBF measurements of clusters younger than 5 Gyr appear in agreement with models of metallicities $Z = 0.004$–0.01, which are appropriate for young and intermediate-age LMC clusters (e.g., Westerlund 1997; MG03). SBF measurements for very old clusters are fitted by 12–15 Gyr with lower metallicity models.

For I-band SBFs (Fig. 9*b*) the agreement is still good in the case of measurements with small uncertainties. Some relevant discrepancies arise for NGC 1868, NGC 2209, and Hodge 14. Let us recall that the three quoted clusters have the faintest integrated light in our sample; thus, statistical effects may be not negligible as inferred from Figure 2 (§ 3.1). We also remind the reader that in order to avoid contamination by field stars, in the case of Hodge 14 only a small fraction (i.e., a small mass) of the cluster is being analyzed. This indication is confirmed if detailed models are computed by assuming exactly the integrated magnitude and age reported in Table 3 (cols. [3] and [7]). The I-band SBFs, derived by applying the RS procedure ($\bar{M}_I^{\rm RS}$), provide values that are lower than $\bar{M}_I^{\rm std,\,as}$ and closer to the observed ones. In fact, for NGC 1868, NGC 2209, and Hodge 14 we find, respectively, $\bar{I}^{\rm RS} = 16.6 \pm 0.5$, 16.4 ± 1.0, and 16.5 ± 0.9, which can be compared to the corresponding asymptotic values $\bar{I}^{\rm std,\,as} = 15.93 \pm 0.05$, 15.84 ± 0.05, and 16.06 ± 0.05. Note that similar computations performed for the massive cluster NGC 1866 give $\bar{I}^{\rm RS} = 15.0 \pm 0.1$. SBFs in the V band show a similar behavior, in the sense that the agreement gets even better if $\bar{M}_V^{\rm RS}$ values are compared to observations. Statistical effects are mainly driven by fluctuations in the number of giant stars, and then for intermediate-age/old populations they affect the I and NIR bands more than the optical ones (Fig. 2).

Even with the present large error bars and the limited sample of LMC clusters we are dealing with, we can reach the following conclusions:

1. SSP models including TP stars reproduce the optical SBFs of LMC clusters reasonably well. This rules out an extremely high mass loss rate, thus driving stars to an early departure from the AGB.
2. A mild mass loss rate (BH83) appears inadequate, because too many TP stars are foreseen. SSPs predict a very "red" ($\bar{V} - \bar{I}$) color, which is not supported by the observed SBF values.
3. B1 and B2 models seem to predict a number of TP stars that can reproduce the SBFs of the selected sample of LMC clusters.

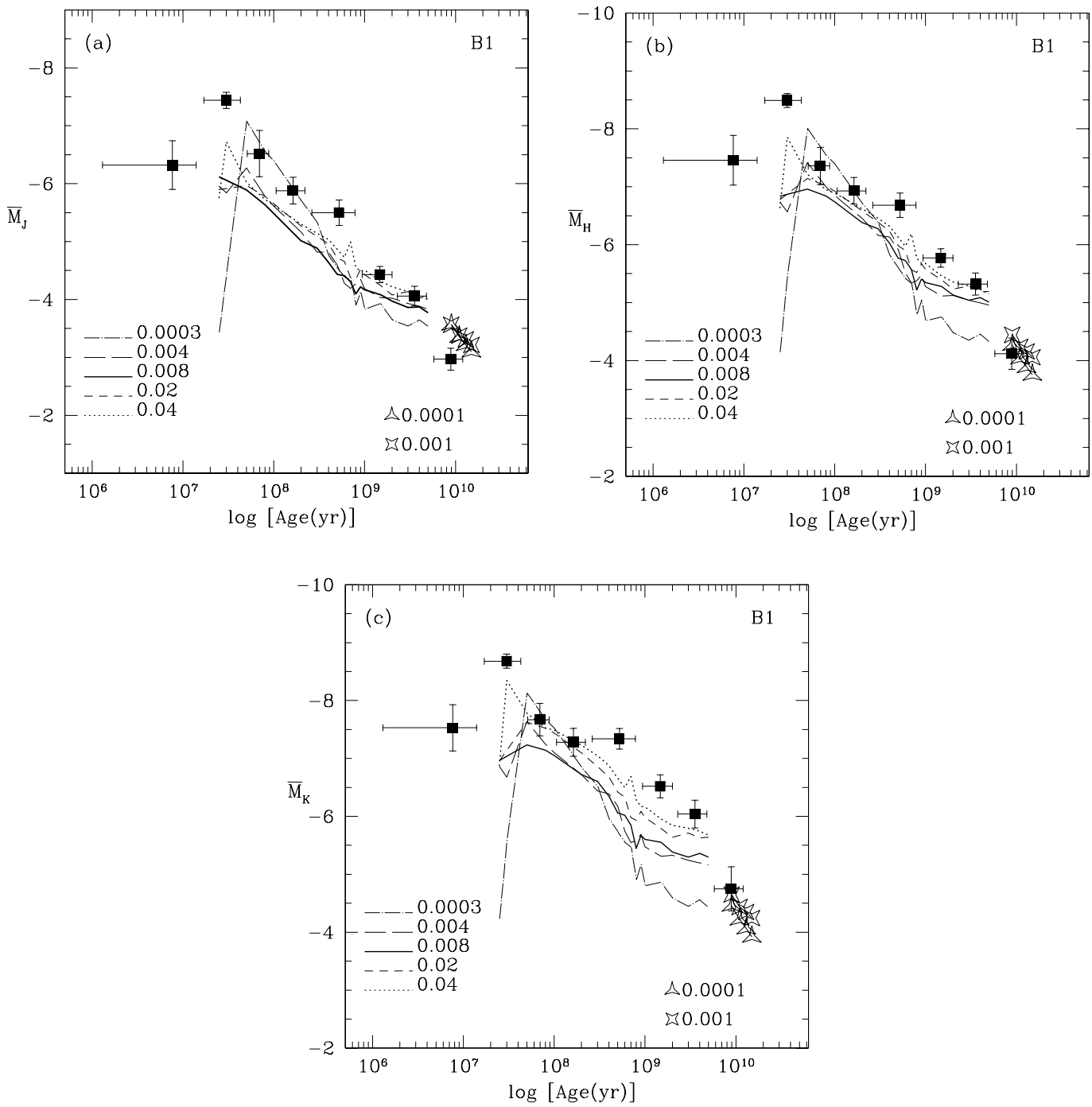

FIG. 10.—*JHK* SBF predictions of B1 models for selected values of metallicity as a function of age. Models for $t > 5$ Gyr are from Paper I (symbols as in Fig. 8). The SBFs of MC superclusters by G04 are plotted as filled squares. Age uncertainties cover the interval spanned by each SWB class according to the *s*-parameter values included in the superclusters. [*See the electronic edition of the Journal for a color version of this figure.*]

Due to the relatively small number of LMC clusters included in our sample, the previous conclusions must be regarded as important, although not conclusive, indications. Further observational efforts are requested, both in improving the size of the sample and in minimizing the uncertainties of the measurements.

5.2. *NIR SBF*

G04 recently provided *JHK* SBF measurements of eight superclusters as obtained from 2MASS observations of several LMC and Small Magellanic Cloud (SMC) stellar clusters. Each supercluster groups clusters within a given range of the *s*-parameter (Elson & Fall 1985) and corresponds to an SWB class (Searle et al. 1980). The SBFs derived from these superclusters have the remarkable advantage of relying on a large number of bright stars. For this reason, we compared the present models with those NIR data.

Differently from Gonzalez and collaborators, who used the Cohen (1982) ages for the SWB classes, we adopted the age calibration of the *s*-parameter from two more recent works: Elson & Fall (1988) and Girardi et al. (1995). They provide similar results (within 5%–10%) even though one is based on *canonical* stellar models ($\log t = 6.05 + 0.079s$; Elson & Fall 1988) and the other one on *overshooting* stellar models ($\log t = 6.227 + 0.0733s$; Girardi et al. 1995).

In Figure 10 we plot our *JHK* SBF predictions as a function of age for different metallicities and the B1 models. The observational

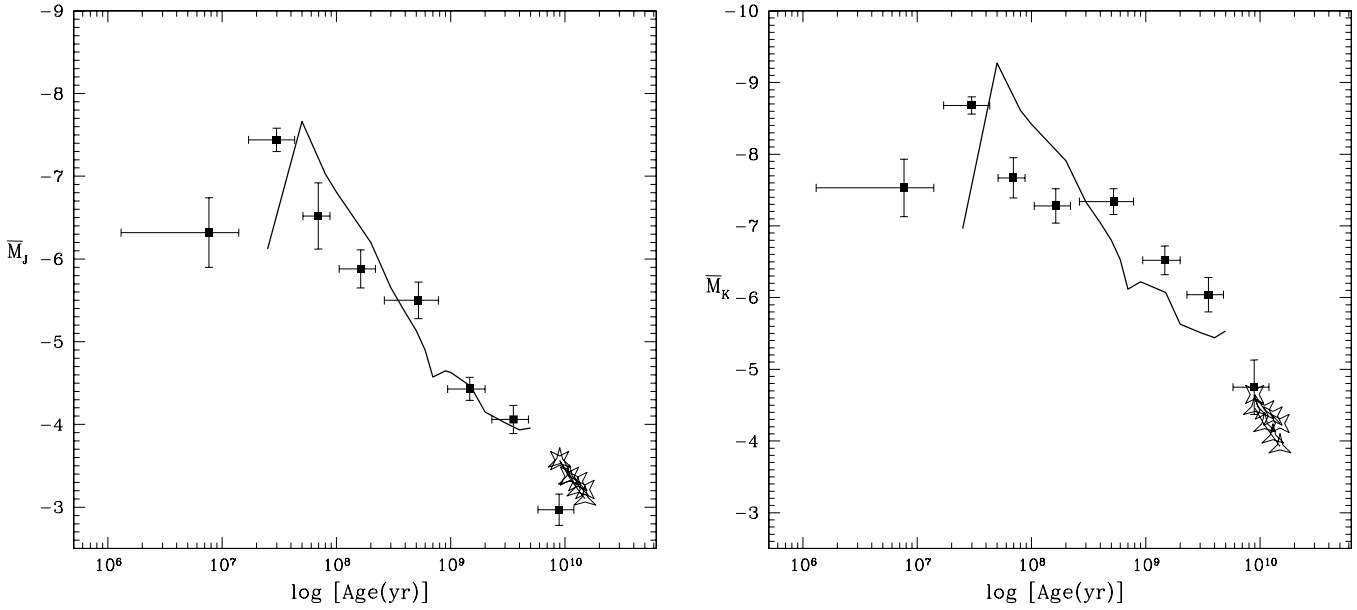

FIG. 11.—*J*- and *K*-band SBF predictions obtained by BH models and metallicity $Z = 0.008$ (*solid line*). Models for $t > 5$ Gyr are from Paper I ($Z = 0.0001$, *three-pointed stars*; $Z = 0.001$, *four-pointed stars*). [*See the electronic edition of the Journal for a color version of this figure.*]

data published by G04 (as corrected after Gonzalez et al. 2005) are reported as filled squares, with the related ages according to the canonical calibration. The age error bars refer to the ages corresponding to the initial and final *s*-parameter values of the clusters included in each supercluster. We rescaled G04 measurements to the LMC distance adopted in previous sections. The models are calculated for a slightly different *K*-band filter than the 2MASS *K*-band filter (K_s), but the differences are negligible for our present purpose (Carpenter 2001).

The general behavior of *JHK* SBF data is reproduced by models in all NIR bands. Both models and data show a jump around 30–50 Myr corresponding to the appearance of red and bright AGB stars. After that, the luminosity of the AGB tip decreases with age, and the SBF NIR data decline accordingly. In spite of the qualitative agreement concerning the general trend, the quality of the fit is *not* satisfactory.

The comparison shows that SBFs from B1 models are systematically fainter than NIR SBF magnitudes of the MC superclusters. In the range from a few hundred megayears to a few gigayears, only supersolar SSP models give SBF magnitudes as bright as G04 data. It is well known that MC clusters have chemical abundances lower or at most equal to the solar value, so that metallicity variations do not appear to properly solve the quoted discrepancy. Other models (G04) also require unlikely high values of metallicity to reproduce the SBF measurements obtained for superclusters.

We evaluated the impact of increasing the number of cool bright AGB stars by comparing the supercluster data to the SBF predictions obtained by BH models. Figure 11 (*left*) shows that *J*-band SBF magnitudes seem to be well fitted by BH models with reasonable metallicity values. Unfortunately, these models fail in reproducing *K*-band measurements, since the theoretical SBF amplitudes are brighter than the data for $t \sim 100$ Myr and fainter for older ages (Fig. 11, *right*). Hence, this scenario seems to be ruled out too.

Which kind of stars are missed in the models, and what place should they occupy in the CMD in order to move the theoretical NIR SBF magnitudes to the observed values? Note that SBF predictions in the optical bandpasses should not be affected by including those kinds of stars, because the SBF in that range of wavelength can fit observations. This leads to an investigation of the lack of cool bright stars in our models. In order to reproduce exactly the SBFs of superclusters, we performed numerical experiments by assembling the number of simulations needed to form a supercluster with a total mass $\mathcal{M} \sim 4 \times 10^6\ M_\odot$, representing the average value from classes II–VII of G04 at a given age (B1 models and $Z = 0.008$). Obviously, the SBFs derived for these theoretical superclusters resemble—within the uncertainties—the SBFs reported in Table 1, because we are dealing with asymptotic values.

As a first approximation, we verify what happens to theoretical NIR SBFs if a contamination of LMC supergiant M-type field stars is included (Nikolaev & Weinberg 2000). Figure 3 of G04 shows that a nonnegligible number of bright stars at $K_s \simeq 10$ and $J - K_s \simeq 1$–1.2 are present in the superclusters corresponding to SWB classes I–IV. If such a small contamination of field stars is included into our theoretical superclusters, we find that models shift toward a higher luminosity. Furthermore, the presence of NIR-bright AGB stars displaying ^{12}C enrichment, due to the third dredge-up (C-stars), also affects SBFs in these bands. The K_s versus $J - K_s$ CMDs of the superclusters (Fig. 3 of G04; SWB classes IV, V, and VI) show stars with $J - K \gtrsim 1.3$–1.4, the typical value used to select C-stars photometrically in the SMC and LMC (Cioni et al. 2001, 2003; Raimondo et al. 2005). Cohen (1982) already stated that these classes are "precisely those where integrated light (Persson et al. 1983) and searches among the brightest red stars (Frogel & Cohen 1982; Aaronson & Mould 1982) have revealed the presence of luminous carbon stars." If this is the case, the discrepancy between NIR data and models should be reduced by moving from the *K* to the *J* band and is expected to become negligible in the optical range. This is exactly what happens, as shown in Figure 10. From Figure 3 of G04, we note that SWB classes V and VI show a narrow giant branch with a group of stars redder than $J - K \gtrsim 1.4$, roughly 10 and 4 for SWB classes V and VI, respectively. By adding these stars to our theoretical superclusters, SBF predictions go up to the same position of observational values (Fig. 12).

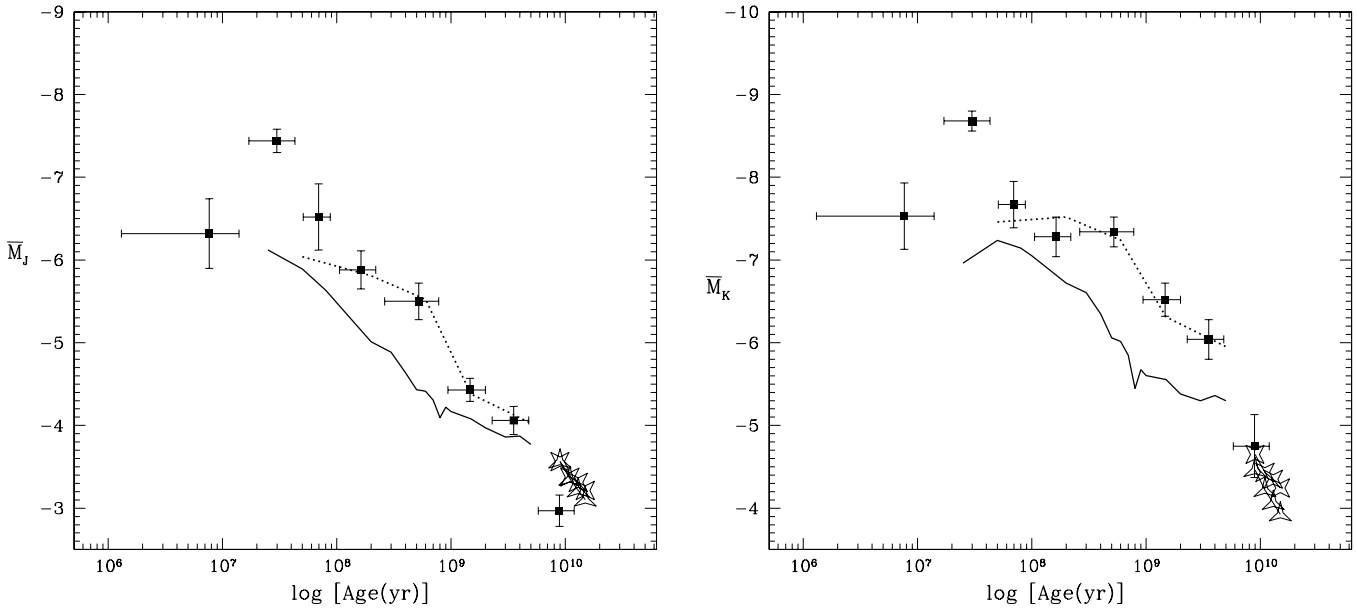

FIG. 12.—*J*- and *K*-band SBF predictions for theoretical superclusters obtained from B1 models by including a contamination of M-type field stars *and* by artificially increasing the number of stars with $J - K \gtrsim 1.3-1.4$ (C-stars?) in the SSPs (*dotted line*). As a reference, the original B1 models with $Z = 0.008$ are shown (*solid line*). Symbols are as in Fig. 11. [*See the electronic edition of the Journal for a color version of this figure*.]

All in all, these numerical experiments lead to the conclusion that models with the proper MC metallicity can be reconciled with the observed NIR SBFs for MC superclusters if (1) a field contamination of M-type stars is assumed, *and* (2) the number of stars with $J - K \gtrsim 1.3-1.4$ is increased in the SSP models.

In spite of the fairly good agreement obtained in Figure 12, we explored a further possibility. Let us recall that superclusters are not really SSPs, being the results of a sum of individual stellar clusters with slightly different ages and chemical compositions. In addition, the membership of an individual cluster to a given SWB class may be uncertain (Girardi et al. 1995). Thus, we investigated the possibility that superclusters contain a certain fraction of populations younger than the minimum age assigned to the corresponding SWB classes. This suggestion is supported by the fact that CMDs of SWB classes I–IV in Figure 3 by G04 exhibit features that could be related to the presence of populations with chemical compositions and/or ages different from the corresponding SWB class (see, e.g., the bimodal RGBs).

Numerical experiments performed for SWB classes from II to VI show a relevant increment of the SBF magnitudes if a stellar population younger than the typical age value assigned to the corresponding SWB class is included. In particular, we find that the presence of one (or a few) younger cluster leads to SBF predictions in agreement with observations (Fig. 13). Keeping in mind that the results in Figure 13 do not represent the only solution, we note that the percentage of young population required to predict the SBF NIR data is on the order of 10%. In other words, if one (or a few) cluster is included in a given SWB class because

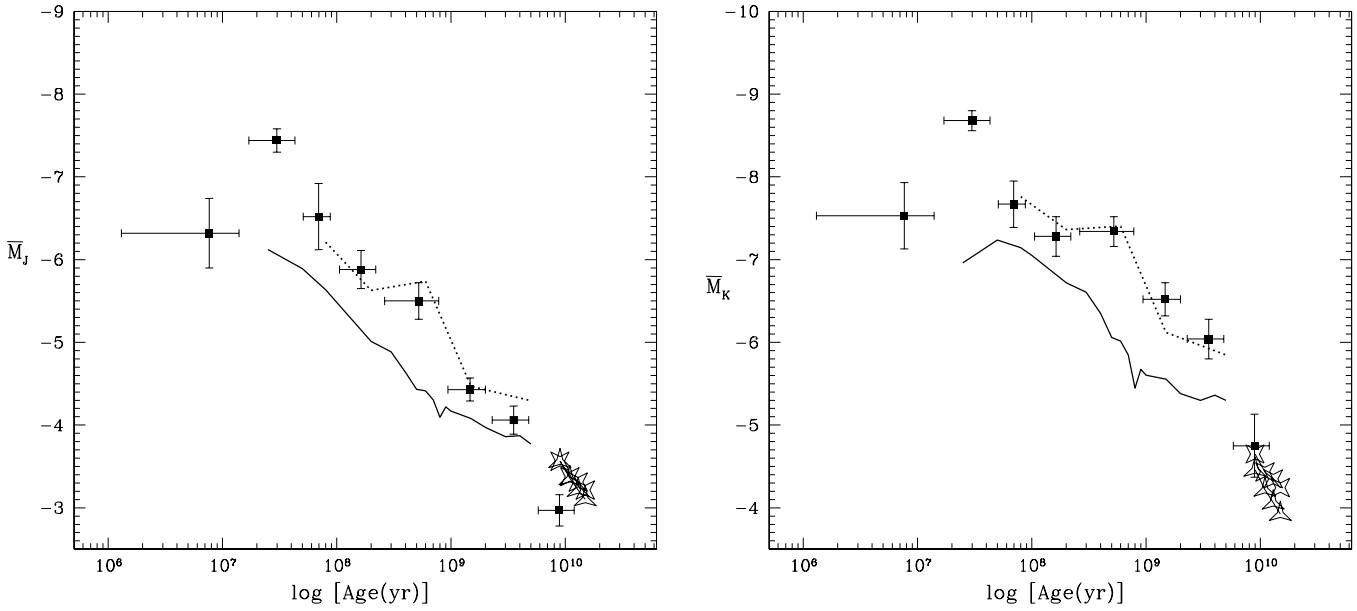

FIG. 13.—*J*- and *K*-band SBFs for composite stellar populations (*dotted line*; see text). Symbols are as in Fig. 11. [*See the electronic edition of the Journal for a color version of this figure*.]

its *s*-parameter is overestimated (for whatever reason; see Girardi et al. 1995), this leads to brighter SBF amplitudes for that SWB class. On the contrary, numerical experiments show that an underestimation of the *s*-parameter of one (or a few) cluster would not significantly affect the supercluster SBF measurements.

In conclusion, we showed that the NIR SBFs of the superclusters by G04 can be reproduced, although not in a definitive way. Further observational and theoretical efforts are required to improve the understanding of NIR SBF amplitudes of young and intermediate-age stellar populations.

6. SUMMARY AND CONCLUSIONS

We presented new theoretical SBF amplitudes for single-burst stellar populations of young and intermediate age (25 Myr $\leq t \leq 5$ Gyr) and metallicity ranging from $Z = 0.0003$ up to 0.04. The new SBF models are based on an updated version of the stellar population synthesis code already used to derive SBFs for old stellar populations in Paper I. In the present version of the code, we used the recently published evolutionary tracks database of P04 and $T_{\rm eff}$ color relations from Westera et al. (2002). Particular care has been given to the simulation of the properties of intermediate-mass AGB stars experiencing the TP phase. The time evolution of core mass and luminosity, together with the overall evolutionary timescale of these stars, have been evaluated according to prescriptions by WG98. In addition, the number of TP-AGB stars is also determined by mass-loss efficiency. Therefore, in order to evaluate the impact of this type of star on fluctuation amplitudes, three different mass-loss scenarios were simulated (BH, B1, and B2), along with the extreme case of no TP stars at all.

The resulting new database of stellar population models covers a wide range of chemical compositions and ages. The accurate SSP models allowed us to successfully fit the observed CMD features of a sample of LMC star clusters imaged with the *HST* WFPC2 (*V* and *I* bands). Age, metallicity, and reddening for all clusters are derived and successfully compared with literature estimations.

Owing to the Monte Carlo technique, which is the basis of our method to derive fluctuation amplitudes, we estimated the cluster integrated magnitude $M_V^{\rm tot}$ required to minimize uncertainty caused by stochastic effects due to random variation of the number of bright stars affecting SBF measurements. We find that the procedure used to compute SBFs from individual stars of a synthetic CMD (RS procedure) provides—within uncertainties—the same results as the standard procedure if $M_V^{\rm tot} \lesssim M_V^{\rm tot,\,max}$, where $M_V^{\rm tot,\,max}$ is a function of the stellar population age and metallicity. This has a direct application in the observational field. First, once the absolute integrated magnitude of the measured sample of stars is known, the RS procedure provides a tool to evaluate the intrinsic uncertainty of SBF measurements as derived by individual-star photometry of a real stellar system (Fig. 2). Second, the SBFs derived from the photometry of spatially resolved systems can be compared properly with the theoretical SBF asymptotic values only if the stellar system integrated magnitude satisfies the condition $M_V^{\rm tot} \lesssim M_V^{\rm tot,\,max}$; otherwise, stochastic effects prevent a reliable and meaningful comparison.

By focusing the attention on optical SBFs, we performed the first *V*- and *I*-band SBF measurements for 11 LMC clusters using *HST* WFPC2 photometry of individual stars. The explored ages range from $\sim$10 Myr, for the very young cluster NGC 1805, up to the typical age of GGCs (NGC 1754, 1916, 2005, and 2019). The comparison of SBF measurements with our models showed a good agreement with both observed fluctuation magnitudes and colors if metallicities of $Z = 0.008$–0.01 and 0.001–0.0001 were adopted, respectively, for young/intermediate-age and very old clusters. The $(\bar{V} - \bar{I})$ fluctuation color has been found to be sensitive to the adopted mass-loss scenario along the TP phase. The comparison between SBF models and measurements suggests that B95 mass-loss rates better simulate the observed LMC cluster fluctuation colors.

Few interesting features have been identified in the time-evolution behavior of fluctuation magnitudes and colors of the present models. Sizable variations arise at $t \sim 50$ Myr and $t \sim 1$ Gyr. These jumps correlate with the RGB and AGB phase transitions. For stellar populations younger than 1 Gyr the high sensitivity exhibited by SBF magnitudes to age variation supports the use of the SBF tool to evaluate ages of young stellar clusters in Local Group galaxies.

The capability of the stellar population synthesis code to directly manage parameters and physical processes characterizing the TP-AGB evolutionary phase allows us to analyze in depth the SBF dependence on TP-AGB stars. It is worth remarking that the different mass-loss scenarios affect both SBF magnitudes and colors for populations older than 1 Gyr only for a few tenths of magnitudes, confirming the results given in Paper I. On the other hand, for $t < 1$ Gyr the SBF amplitudes appear to be highly dependent on the adopted mass-loss scenario. Therefore, in this age range SBFs can be used to infer information on the mass-loss efficiency of both resolved and unresolved young stellar populations.

The comparison with NIR SBF observations of MC superclusters has shown that our models reproduce the general trend of the data, but a deeper analysis discloses that unlikely high values of metallicity are required to fit the supercluster data. We have shown that composite stellar populations or contamination by field stars coupled with more precise simulations of very cool stars (C-stars) may reconcile NIR SBFs of MC superclusters with theoretical predictions.

Therefore, SBF studies in both the optical and NIR regime give evidence that further theoretical and observational efforts are needed to improve the models' accuracy and the reliability of measurements for nearby well-known objects. On the other hand, the SBF technique should be regarded as a very valuable tool for improving our knowledge of unresolved stellar populations in distant galaxies for which SBF measurements can be used to detect the presence of young and intermediate-age stellar populations and to investigate their evolutionary properties more efficiently than "classical" integrated light studies.

We thank R. González-Lópezlira for providing constructive and insightful comments that have greatly improved the paper. It is a pleasure to acknowledge Adriano Pietrinferni and Santi Cassisi for providing evolutionary tracks and S. Shore for useful discussions and for a careful reading of the manuscript. Financial support for this work was provided by MIUR-Cofin 2003. This work made use of computational resources granted by the Consorzio di Ricerca del Gran Sasso according to the Progetto 6 "Calcolo Evoluto e sue Applicazioni (RSV6)"-Cluster C11/B. This paper is based on observations made with the NASA/ESA *Hubble Space Telescope*, obtained from the ESO/ST-ECF Science Archive Facility, and data products from the Two Micron All Sky Survey, which is a joint project of the University of Massachusetts and the Infrared Processing and Analysis Center, California Institute of Technology, funded by the National Aeronautics and Space Administration and the National Science Foundation.

APPENDIX A

MODELING THE TP-AGB STELLAR EVOLUTION PHASE

The present SSP models rely on the evolutionary tracks database by P04, which includes all the most updated physical inputs in computing stellar models, such as, for example, a new equation of state (see Cassisi et al. 2003) and recent nuclear reaction rates by Angulo et al. (1999) and Kunz et al. (2002) for the $^{12}C(\alpha, \gamma)\ ^{16}O$ reaction (see P04 for more details). The database covers a wide range of chemical compositions and stellar masses. Intermediate- and low-mass stellar models end up at the first thermal pulse; thus, the evolution along the TP-AGB phase is not provided. Therefore, in the following we describe the procedure currently adopted to simulate this bright and fast evolutionary phase in our stellar population synthesis models in order to properly compute SBF amplitudes.

Although it is well known that the AGB evolution of stellar masses $m \lesssim 6{-}8\ M_{\odot}$ (depending on metallicity) ends with a series of helium shell flashes or TPs (e.g., Iben & Renzini 1983), a series of difficulties in modeling these stars still arises. These come from several physical mechanisms. Among others, we recall (1) the treatment of convection, which is poorly known and commonly parameterized by the mixing length theory (MLT) with the mixing length scale free parameter (usually indicated as α); (2) the mass-loss rate, for which observations indicate a value ranging from 10^{-7} to even $10^{-3}\ M_{\odot}\ \mathrm{yr}^{-1}$ for the coolest and most luminous red supergiants (Van Loon et al. 1999); (3) the occurrence of hot bottom burning and of the third dredge-up, which regulate the formation of C-stars; and (4) the luminosity variations, which may reach an amplitude on the order of a few magnitudes in V and a few tenths in NIR bands (Cioni et al. 2001; Raimondo et al. 2005). Therefore, fully modeling the TP-AGB phase is indeed complex and time-consuming; thus, stellar population models make use of analytic approaches (WG98; Marigo 1998, hereafter M98).

In intermediate- and low-mass stellar models by P04, the evolution is followed from the MS until the onset of TPs. To extend the track to the TP phase, we used the analytic formulae by WG98, simulating the behavior of each TP-AGB star in terms of its core mass (m_c) and luminosity (L) as a function of time. The adopted relation between the maximum bolometric luminosity L during the quiescent hydrogen burning and the core mass m_c (in solar units) is

$$\begin{aligned} L = {} & (18160 + 3980z)(m_c - 0.4468) \\ & + 10^{2.705+1.649m_c}\left(10^{0.0237(\alpha-1.447)m_{c,0}^2 m_e^2(1-e^{-\Delta m_c/0.01})}\right) \\ & - 10^{3.529\ -\ (m_{c,0}-0.4468)\Delta m_c/0.01}, \end{aligned} \tag{A1}$$

where $z = \log(Z/Z_{\odot})$ refers to the MS metal abundance, $m_{c,0}$ is the core mass at the first thermal pulse, Δm_c is defined as $\Delta m_c = m_c - m_{c,0}$, and m_e is the envelope mass. Concerning the MLT parameter, we assumed $\alpha = 2$ according to the value used by P04 in the previous evolutionary stages.

The equation of the core growth is

$$\frac{dm_c}{dt} = \frac{q}{X_e} L_{\mathrm{H},} \tag{A2}$$

where q is the mass burned per unit energy release,

$$q = [(1.02 \pm 0.04) + 0.017z] \times 10^{-11}\ (M_{\odot}\ L_{\odot}^{-1}\ \mathrm{yr}^{-1}), \tag{A3}$$

X_e is the hydrogen in the envelope (mass fraction), and L_{H} is the luminosity produced by H-burning, which is obtained by

$$\log(L_{\mathrm{H}}/L) = -0.012 - 10^{-1.25-113\Delta m_c} - 0.0016 m_{e.} \tag{A4}$$

Finally, the core mass–interpulse time relation is

$$\begin{aligned} \log \tau_{\mathrm{ip}} = {} & (-3.628 + 0.1337z)(m_c - 1.9454) \\ & - 10^{-2.080-0.353z+0.200(m_e+\alpha-1.5)} \\ & - 10^{-0.626-70.30(m_{c,0}-z)\Delta m_c}. \end{aligned} \tag{A5}$$

We performed an integration of the system of equations, obtaining for each thermal pulse the luminosity, the core mass, and the duration of the pulse. We also included a mass-loss rate regulating the total mass at each TP star, as extensively discussed in § A1. The stellar temperature is derived using the prescription of Renzini & Voli (1981), considering the appropriate slope $d\log(L/L_{\odot})/d\log(T_e)$ for the evolutionary tracks we are using. The procedure ends by providing the "expected" evolution of a star of a given mass during the TP phase.

A1. MASS-LOSS EFFICIENCY FOR TP-AGB STARS

In this work, mass loss is parameterized by following the prescription of Reimers (1975) along the RGB and on the AGB until the first thermal pulse:

$$\dot{m}_R = -4 \times 10^{-13} \eta_R L R/m, \tag{A6}$$

where L, R, and m are respectively the star luminosity, radius, and total mass in solar units; along these phases we assumed $\eta_R = 0.4$.

The quantitative determination of mass-loss rate along the TP phase is a complex problem, since dust formation and circumstellar dust shells preclude in several cases the possibility of observing stars in the optical band. Nevertheless, the duration of the TP phase is determined by the efficiency of the mass loss; thus, to parameterize mass-loss processes we followed several prescriptions. After the first thermal pulse, we first used the formulation by BH83 derived from statistical properties of OH/IR stars:

$$\dot{m}_{\mathrm{BH}} = \mu L R/m_e, \tag{A7}$$

with $\mu = -4 \times 10^{-13}(m_{e,0}/m)$, where $m_{e,0}$ is the envelope mass at the first TP. This is a modification of the Reimers formula with $\eta_R = 1$, which also includes a dependence on the actual mass envelope.

For the sake of clarity, the present TP evolution is compared with the results by other authors. In Table A1 we report the TP evolution of a star with an original MS mass $m_{\mathrm{MS}} = 7\ M_{\odot}$ and solar metallicity, with similar calculations by M98) and Blocker & Schoenberner (1991, hereafter BS91). Table A1 lists the thermal pulse number (col. [1]), the mass of the star (col. [2]), the core mass (col. [3]), and the star luminosity after a certain number of thermal pulses (col. [4]). The first block refers to the TP evolution obtained by adopting the procedure described above, starting from values of luminosity, temperature, and core mass at the first TP according to P04 (case 1). The second block refers to the same TP procedure, but the initial values of luminosity, temperature, and core mass at the first TP are from BS91 (case 2).

TABLE A1
COMPARISON WITH PREVIOUS WORKS

Number (1)	m ($M_\odot$) (2)	m_c ($M_\odot$) (3)	L ($L_\odot$) (4)
Present Procedure (Case 1)			
1	6.928	0.938	33798
10	6.903	0.944	48265
20	6.837	0.953	64887
30	6.674	0.961	73937
Present Procedure (Case 2)			
1	6.871	0.913	25217
10	6.848	0.920	36581
20	6.796	0.930	48570
30	6.728	0.940	54352
BS91			
1	6.871	0.913	25217
10	6.854	0.921	40268
20	6.821	0.930	51662
30	6.774	0.939	58806
M98			
1	6.871	0.913	25217
11	6.850	0.921	37788
22	6.807	0.930	51537
34	6.745	0.939	60760

NOTE.—The BH model mass-loss rate is adopted.

The last two blocks report the TP evolution from BS91 and M98. There is a fair agreement (within ~10% in luminosity) between block 2 and blocks 3 and 4. Larger differences are found if we make use of the stellar models by P04 (case 1). This case foresees stars experiencing the TP stage at a level brighter than that found by M98 and BS91 (e.g., ~25% at TP 30). Note that for the given mass ($m_{\rm MS} = 7\,M_\odot$), tracks by P04 predict a higher luminosity at the first TP than those adopted by M98 and BS91.

As shown by B95, the BH83 formulation cannot well reproduce the observed initial-final mass relationship. He proposed a mass-loss rate based on dynamical theoretical investigation of the atmospheres of Mira-like variables by Bowen (1988). B95 suggested two mass-loss rates directly correlated with the stellar luminosity:

$$\dot{m}_{\rm B1} = 4.83 \times 10^{-9} m_{\rm MS}^{-2.1} L^{2.7} \dot{m}_R, \quad \text{(A8)}$$

$$\dot{m}_{\rm B2} = 4.83 \times 10^{-9} m_{\rm TP}^{-2.1} L^{2.7} \dot{m}_R, \quad \text{(A9)}$$

with $\eta_R = 1$. These formulas are valid for long-period variable stars with periods $P > 100$ days. They differ in the adopted stellar mass: case B1 makes use of the MS mass ($m_{\rm MS}$), while B2 uses the actual mass ($m_{\rm TP}$), predicting a steeper increase of the mass-loss rate. As an example, in the range of stellar masses we are interested in, the foreseen mass-loss rates in the case of $m_{\rm MS} = 5\,M_\odot$, $Z = 0.02$ and at the luminosity level $L \simeq 19{,}600\,L_\odot$ are $\dot{m} \simeq 6 \times 10^{-6}\,M_\odot$ yr^{-1} in the BH83 case, $\dot{m} \simeq 4.4 \times 10^{-5}\,M_\odot$ yr^{-1} for B1, and $\dot{m} \simeq 8.5 \times 10^{-5}\,M_\odot$ yr^{-1} in the B2 case. The B95 scenarios foresee more efficient mass-loss rates than BH83, predicting a lower number of stars and a shorter lifetime along the TP phase. The high sensitivity of SBFs to mass loss is shown in § 3.2, in which we suggest that SBFs might be used as calibrators of mass-loss rates for young and intermediate-age stellar populations, as for old stellar systems (Paper I).

APPENDIX B

ABOUT THE STOCHASTIC EFFECTS ON SBF MEASUREMENTS

In order to deepen the investigation of stochastic effects due to variations of the number of bright stars, we performed numerical experiments by varying the stellar population total mass $\mathcal{M}$. Figures 14*a*, 14*c*, and 14*e* illustrate how *I*-band SBF amplitude is affected by stochastic effects depending on the star cluster richness, as a function of $N_{\rm sim}$. Solid (red) lines refer to SBFs derived using the standard procedure based on integrated fluxes [eq. (1); $\bar{M}_I^{\rm std}(N_{\rm sim})$]; dots represent SBFs derived from the RS procedure with the jth simulation (eq. [4]; $\bar{M}_I^{{\rm RS},j}$). We consider SSPs with $t = 100$ Myr and $Z = 0.008$. The total mass increases from the top to the bottom.

First of all we focus the attention on $\bar{M}_I^{{\rm RS},j}$. For small values of the SSP mass, stars belong typically to the MS, as indicated by the corresponding CMD (Fig. 14*b*). Due to the small number of stars, only a few simulations have a few occasional stars burning He in the core, and even fewer simulations have the odd AGB stars. Correspondingly, $\bar{M}_I^{{\rm RS},j}$ is dominated by MS stars (Fig. 14*a*, *the bulk of dots at* $\bar{M}_I^{{\rm RS},j} \sim -1$ mag). When a few He-burning stars appear in the CMD, the *I*-band SBF becomes brighter ($\bar{M}_I^{{\rm RS},j} \sim -3$ mag), and even brighter if a TP-AGB star appears in the simulation ($\bar{M}_I^{{\rm RS},j} \sim -6.5$ mag, *the few five-pointed stars*).

By increasing the stellar population mass, the number of He-burning stars and AGB stars grows in the CMD: first the He-burning phase (Heb) becomes well populated (Fig. 14*d*), then, for a further increase of the total mass, a large number of stars populates the AGB and TP-AGB phases (Fig. 14*f*). Correspondingly, the SBF signal is always dominated by those evolved stars (Figs. 14*c* and 14*e*). Therefore, the scatter of the SBF signal inversely correlates with the stellar population mass $\mathcal{M}$: $\bar{M}_I^{{\rm RS},j}$ brighter than -5 mag is never produced by SSPs with $\mathcal{M} = 2.5 \times 10^5\,M_\odot$, while a few simulations among SSPs with $\mathcal{M} = 5 \times 10^2\,M_\odot$ can reach $\bar{M}_I \sim -6.5$ mag. The reason is that for lower $\mathcal{M}$, the fluctuation for the few simulations with bright stars is larger than the fluctuation of the typical simulation without bright stars.

The red solid lines in Figure 14 (*left panels*) illustrate how the SBF signal derived using the standard procedure becomes stable with $N_{\rm sim}$ approaching the asymptotic value. Discontinuities in the solid lines are directly related to the appearance of one or more very bright stars in the simulation (e.g., Fig. 14*a*). By increasing the total mass of the population, this event occurs with a higher probability, and discontinuities tend to disappear. If we add stars to the population, we obtain a *faster* convergence of $\bar{M}_I^{{\rm RS},j}$ to the asymptotic value, $\bar{M}_I^{\rm std,as}$ (Figs. 14*c* and 14*e*).

Before closing this Appendix, let us make a further consideration of Figure 14. From the figure one can note that $\bar{M}_I^{\rm std}$ already tends to converge rapidly to the asymptotic value after $N_{\rm sim} \sim 500$ simulations, when $\mathcal{M}_{\rm tot} \geq 5 \times 10^3\,M_\odot$. However, even in the case of very poorly populated clusters (Fig. 14*a*), this happens before 2000 simulations. This feature has an important implication for the SBF measurements of unresolved populations in distant galaxies. In fact, the standard procedure approaches the observational way of deriving SBFs in the case of unresolved stellar populations. In such cases the integrated flux we compute for each jth simulation corresponds to the flux measured in a

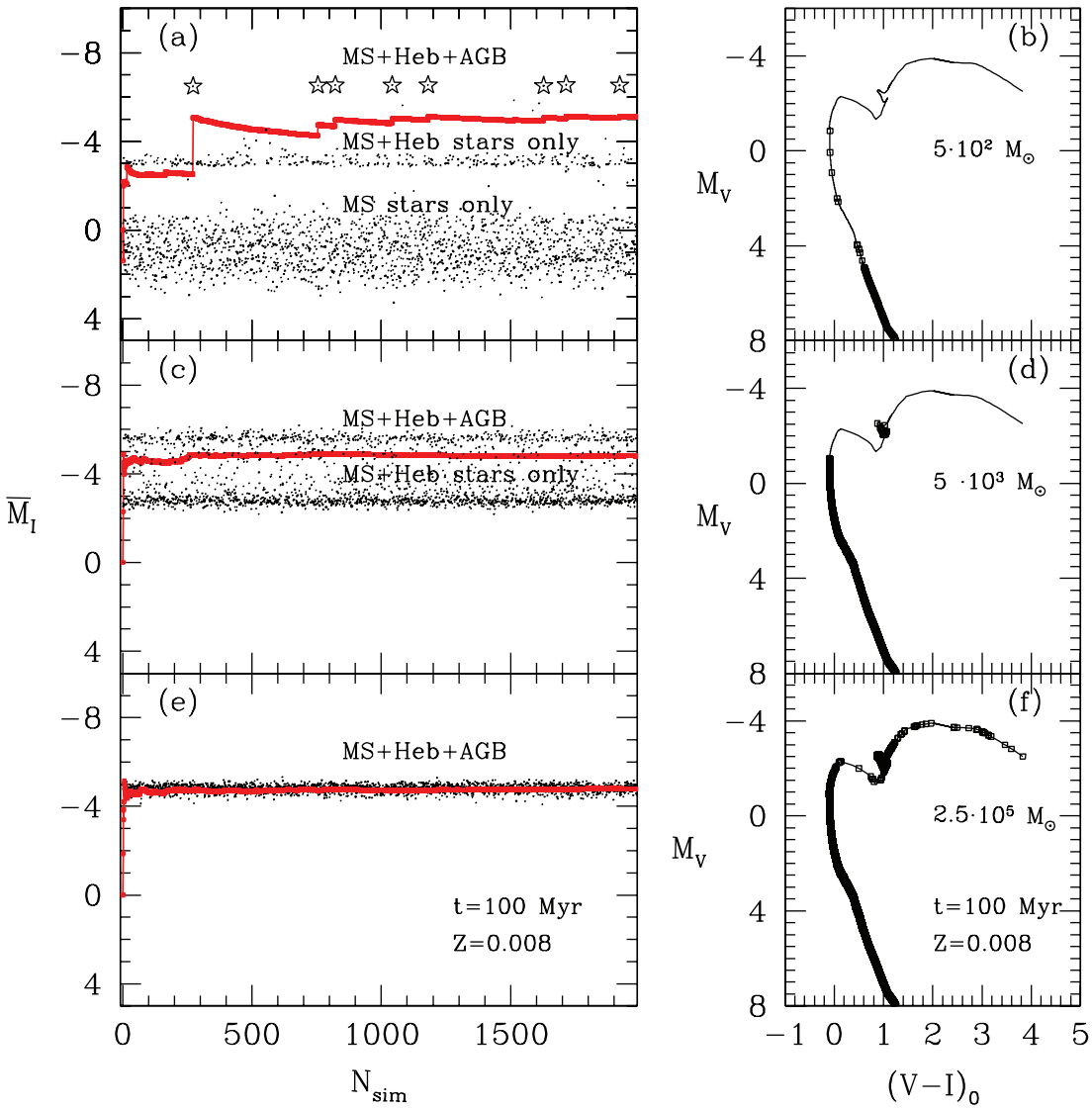

FIG. 14.—(*a*, *c*, *e*) $\bar{M}_I$ for a population of 100 Myr age and with $Z = 0.008$, as a function of the simulation number N_{sim}. The total mass of the stellar population increases from top to bottom: (*a*) $\mathcal{M}_{tot} = 5 \times 10^2\ M_\odot$; (*c*) $\mathcal{M}_{tot} = 5 \times 10^3\ M_\odot$; and (*e*) $\mathcal{M}_{tot} = 2.5 \times 10^5\ M_\odot$. The red solid lines refer to SBFs computed from the standard procedure. Alternatively, each dot represents the SBF as derived from the *j*th synthetic CMD ($\bar{M}_I^{RS,j}$, RS procedure). In (*a*) the five-pointed stars at $\bar{M}_I^{RS,j} \sim -6.5$ mag show the few simulations in which a few AGB stars are also occasionally present in the CMD. (*b*, *d*, *f*) Typical distribution of stars (*squares*) in the synthetic CMD for the labeled total mass and the corresponding isochrone (*solid lines*). The total masses are the same as in the corresponding left panels.

single pixel of a distant galaxy image (if one neglects seeing and population mixture). Within the limit of this approximation, we find that—after cleaning processes (masking, galaxy subtraction, etc.)—the effective number of pixels used in deriving SBF measurements from a galaxy CCD image should be larger than 2000 if one intends to detect the presence of a young stellar population with a mass density lower than $10^3\ M_\odot$ pixel^{-1}. In the case of higher density (e.g., $\gtrsim 10^4\ M_\odot$ pixel^{-1}), the constraint becomes less severe, and 500 pixels are enough to measure SBFs with an uncertainty lower than 0.1 mag.

REFERENCES

Aaronson, M., & Mould, J. 1982, ApJS, 48, 161
Ajhar, E. A., & Tonry, J. L. 1994, ApJ, 429, 557 (AT94)
Alcock, C., et al. 2004, AJ, 127, 334
Angulo, C., et al. 1999, Nucl. Phys. A, 656, 3
Baud, B., & Habing, H. J. 1983, A&A, 127, 73 (BH83)
Blakeslee, J. P., Vazdekis, A., & Ajhar, E. A. 2001, MNRAS, 320, 193
Blocker, T. 1995, A&A, 297, 727 (B95)
Blocker, T., & Schoenberner, D. 1991, A&A, 244, L43 (BS91)
Bowen, G. H. 1988, ApJ, 329, 299
Brocato, E., Capaccioli, M., & Condelli, M. 1998, Mem. Soc. Astron. Italiana, 69, 155
Brocato, E., Castellani, V., Di Carlo, E., Raimondo, G., & Walker, A. R. 2003, AJ, 125, 3111
Brocato, E., Castellani, V., Poli, F. M., & Raimondo, G. 2000, A&AS, 146, 91
Brocato, E., Castellani, V., Raimondo, G., & Romaniello, M. 1999, A&AS, 136, 65
Buzzoni, A. 1993, A&A, 275, 433
Cantiello, M., Blakeslee, J. P., Raimondo, G., Mei, S., Brocato, E., & Capaccioli, M. 2005, ApJ, 634, 239
Cantiello, M., Raimondo, G., Brocato, E., & Capaccioli, M. 2003, AJ, 125, 2783 (Paper I)
Carpenter, J. M. 2001, AJ, 121, 2851
Cassisi, S., Salaris, M., & Irwin, A. W. 2003, ApJ, 588, 862
Castellani, V., Degl'Innocenti, S., Marconi, M., Prada Moroni, P. G., & Sestito, P. 2003, A&A, 404, 645

Cioni, M.-R. L., Marquette, J.-B., Loup, C., Azzopardi, M., Habing, H. J., Lasserre, T., & Lesquoy, E. 2001, A&A, 377, 945
Cioni, M.-R. L., et al. 2003, A&A, 406, 51
Cohen, J. G. 1982, ApJ, 258, 143
de Grijs, R., Gilmore, G. F., Johnson, R. A., & Mackey, A. D. 2002a, MNRAS, 331, 245
de Grijs, R., Gilmore, G. F., Mackey, A. D., Wilkinson, M. I., Beaulieu, S. F., Johnson, R. A., & Santiago, B. X. 2002b, MNRAS, 337, 597
de Grijs, R., Johnson, R. A., Gilmore, G. F., & Frayn, C. M. 2002c, MNRAS, 331, 228
Dolphin, A. E. 2000a, PASP, 112, 1383
———. 2000b, PASP, 112, 1397
Elson, R. A. W., & Fall, S. M. 1985, ApJ, 299, 211
———. 1988, AJ, 96, 1383
Frogel, J. A., & Cohen, J. G. 1982, ApJ, 253, 580
Girardi, L., Bressan, A., Bertelli, G., & Chiosi, C. 2000, A&AS, 141, 371
Girardi, L., Chiosi, C., Bertelli, G., & Bressan, A. 1995, A&A, 298, 87
Gonzalez, R. A., Liu, M. C., & Bruzual A., G. 2003, poster paper presented at Stellar Populations 2003
———. 2004, ApJ, 611, 270 (G04)
———. 2005, ApJ, 621, 557
Groenewegen, M. A. T., Smith, C. H., Wood, P. R., Omont, A., & Fujiyoshi, T. 1995, ApJ, 449, L119
Herwig, F., Blocker, T., Schoenberner, D., & El Eid, M. 1997, A&A, 324, L81
Iben, I., Jr., & Renzini, A. 1983, ARA&A, 21, 271
Jensen, J. B., Tonry, J. L., Barris, B. J., Thompson, R. I., Liu, M. C., Rieke, M. J., Ajhar, E. A., & Blakeslee, J. P. 2003, ApJ, 583, 712
Kunz, R., Fey, M., Jaeger, M., Mayer, A., Hammer, J. W., Staudt, G., Harissopulos, S., & Paradellis, T. 2002, ApJ, 567, 643
Lejeune, T., Cuisinier, F., & Buser, R. 1997, A&AS, 125, 229
Liu, M. C., Charlot, S., & Graham, J. R. 2000, ApJ, 543, 644
Liu, M. C., Graham, J. R., & Charlot, S. 2002, ApJ, 564, 216
Mackey, A. D., & Gilmore, G. F. 2003, MNRAS, 338, 85 (MG03)
Marigo, P. 1998, A&A, 340, 463 (M98)
Marigo, P., Girardi, L., & Chiosi, C. 2003, A&A, 403, 225
Mei, S., Quinn, P. J., & Silva, D. R. 2001, A&A, 371, 779
Nikolaev, S., & Weinberg, M. D. 2000, ApJ, 542, 804
Olsen, K. A. G., Hodge, P. W., Mateo, M., Olszewski, E. W., Schommer, R. A., Suntzeff, N. B., & Walker, A. R. 1998, MNRAS, 300, 665
Pagel, B. E. J., & Edmunds, M. G. 1981, ARA&A, 19, 77
Pahre, M. A., et al. 1999, ApJ, 515, 79
Persson, S. E., Aaronson, M., Cohen, J. G., Frogel, J. A., & Matthews, K. 1983, ApJ, 266, 105
Pietrinferni, A., Cassisi, S., Salaris, M., & Castelli, F. 2004, ApJ, 612, 168 (P04)
Pols, O. R., & Tout, C. A. 2001, Mem. Soc. Astron. Italiana, 72, 299
Raimondo, G., Brocato, E., Cantiello, M., & Capaccioli, M. 2003, poster paper presented at Stellar Populations 2003
Raimondo, G., Cantiello, M., Brocato, E., & Capaccioli, M. 2004, Mem. Soc. Astron. Italiana, 75, 198
Raimondo, G., Cioni, M. R. L., Rejkuba, M., & Silva, D. R. 2005, A&A, 438, 521
Reimers, D. 1975, in Problems in Stellar Atmospheres and Envelopes, ed. A. Unsöld et al. (New York: Springer), 229
Renzini, A., & Buzzoni, A. 1986, in Spectral Evolution of Galaxies, ed. C. Chiosi & A. Renzini (Dordrecht: Reidel), 195
Renzini, A., & Voli, M. 1981, A&A, 94, 175
Salaris, M., Percival, S., Brocato, E., Raimondo, G., & Walker, A. R. 2003, ApJ, 588, 801
Santos, J. F. C., Jr., & Frogel, J. A. 1997, ApJ, 479, 764
Scalo, J. M. 1998, in ASP Conf. Ser. 142, The Stellar Initial Mass Function, ed. G. Gilmore & D. Howell (San Francisco: ASP), 201
Searle, L., Wilkinson, A., & Bagnuolo, W. G. 1980, ApJ, 239, 803
Sodemann, M., & Thomsen, B. 1995, AJ, 110, 179
Stephens, A. W., et al. 2001, AJ, 121, 2584
Straniero, O., Chieffi, A., Limongi, M., Busso, M., Gallino, R., & Arlandini, C. 1997, ApJ, 478, 332
Tonry, J. L., Dressler, A., Blakeslee, J. P., Ajhar, E. A., Fletcher, A. B., Luppino, G. A., Metzger, M. R., & Moore, C. B. 2001, ApJ, 546, 681
Tonry, J. L., & Schneider, D. P. 1988, AJ, 96, 807 (TS88)
van den Bergh, S. 1981, A&AS, 46, 79
Van Loon, J. T., Groenewegen, M. A. T., de Koter, A., Trams, N. R., Waters, L. B. F. M., Zijlstra, A. A., Whitelock, P. A., & Loup, C. 1999, A&A, 351, 559
Wagenhuber, J., & Groenewegen, M. A. T. 1998, A&A, 340, 183 (WG98)
Walker, A. R., Raimondo, G., Di Carlo, E., Brocato, E., Castellani, V., & Hill, V. 2001, ApJ, 560, L139
Westera, P., Lejeune, T., Buser, R., Cuisinier, F., & Bruzual, G. 2002, A&A, 381, 524
Westerlund, B. E. 1997, The Magellanic Clouds (Cambridge: Cambridge Univ. Press)
Westerlund, B. E., Azzopardi, M., Rebeirot, E., & Breysacher, J. 1991, A&AS, 91, 425
Worthey, G. 1993, ApJ, 415, L91